Title: Decoding Heterogenous Single-cell Perturbation Responses

One sentence summary: We present a method to quantify diverse perturbation responses and discover novel biological insights in single-cell perturbation datasets.

Bicna Song[1,2], Dingyu Liu[3,4], Weiwei Dai[5,6], Natalie McMyn[5], Qingyang Wang[7], Dapeng Yang[3], Adam Krejci[8], Anatoly Vasilyev[8], Nicole Untermoser[8], Anke Loregger[8], Dongyuan Song[9], Breanna Williams[3], Bess Rosen[3,10], Xiaolong Cheng[1,2], Lumen Chao[1,2], Hanuman T. Kale[3], Hao Zhang[5], Yarui Diao[11], Tilmann Bürckstümmer[8], Jenet M. Siliciano[5], Jingyi Jessica Li[7,9,12-14,], Robert Siliciano[5,6], Danwei Huangfu[3], Wei Li[1,2,#]

1 Center for Genetic Medicine Research, Children's National Hospital, Washington DC, USA
2 Department of Genomics and Precision Medicine, George Washington University, Washington DC, USA
3 Developmental Biology Program, Sloan Kettering Institute, New York City, NY, USA
4 Louis V. Gerstner Jr. Graduate School of Biomedical Sciences, Memorial Sloan Kettering Cancer Center, New York City, NY, USA.
5 Department of Medicine, Johns Hopkins University School of Medicine, Baltimore, MD, USA
6 Howard Hughes Medical Institute, Johns Hopkins University School of Medicine, Baltimore, MD, USA.
7 Department of Statistics and Data Science, University of California, Los Angeles, CA, USA
8 Myllia Biotechnology GmbH. Am Kanal 27, 1110 Vienna Austria.
9 Bioinformatics Interdepartmental Ph.D. Program, University of California, Los Angeles, CA, USA
10 Weill Cornell Graduate School of Medical Sciences, Weill Cornell Medicine, New York, NY, USA.
11 Department of Cell Biology, Duke University Medical Center, Durham, NC, USA
12 Department of Human Genetics, University of California, Los Angeles, CA, USA
13 Department of Biostatistics, University of California, Los Angeles, CA, USA
14 Department of Computational Medicine, University of California, Los Angeles, CA, USA

Correspondences should be addressed. wli2@childrensnational.org;

Keywords: Perturb-seq, CRISPR-based genetic perturbations, single-cell RNA-seq, computational model

Abstract

Understanding diverse responses of individual cells to the same perturbation is central to many biological and biomedical problems. Current methods, however, do not precisely quantify the strength of perturbation responses and, more importantly, reveal new biological insights from heterogeneity in responses. Here we introduce the perturbation-response score (PS), based on constrained quadratic optimization, to quantify diverse perturbation responses at a single-cell level. Applied to single-cell transcriptomes of large-scale genetic perturbation datasets (e.g., Perturb-seq), PS outperforms existing methods for quantifying partial gene perturbation responses. In addition, PS presents two major advances. First, PS enables large-scale, single-cell-resolution dosage analysis of perturbation, without the need to titrate perturbation strength. By analyzing the dose-response patterns of over 2,000 essential genes in Perturb-seq, we identify two distinct patterns, depending on whether a moderate reduction in their expression induces strong downstream expression alterations. Second, PS identifies intrinsic and extrinsic biological determinants of perturbation responses. We demonstrate the application of PS in contexts such as T cell stimulation, latent HIV-1 expression, and pancreatic cell differentiation. Notably, PS unveiled a previously unrecognized, cell-type-specific role of coiled-coil domain containing 6 (CCDC6) in guiding liver and pancreatic lineage decisions, where CCDC6 knockouts drive the endoderm cell differentiation towards liver lineage, rather than pancreatic lineage. The PS approach provides an innovative method for dose-to-function analysis and will enable new biological discoveries from single-cell perturbation datasets.

Introduction

Perturbation is essential for understanding the functions of the mammalian genome that encodes protein-coding genes and non-coding elements (e.g., enhancers). Single-cell profiling of cells undergoing genetic, chemical, environmental or mechanical perturbations is commonly used to examine perturbation responses at the single-cell level. Recently, high-throughput approaches of perturbation have been developed using single-cell RNA-seq (scRNA-seq) readout, including multiplexing of perturbations and single-cell CRISPR screen (e.g., Perturb-seq, CROP-seq)[1–7]. This concept has been extended to study changes in single-cell chromatin accessibility[8,9], spatial transcriptomics[10] upon perturbations or perturbation combinations[11–13], and other phenomena.

Understanding how perturbations lead to different responses within cells is critical to understanding the fundamental biology behind perturbation. Technical factors, including single-cell assays used to profile the response, and the on-target/off-target effects of perturbations, are known drivers that lead to differences of single-cell profiles in the data[14–16]. In Perturb-seq experiments that use CRISPR/Cas9 for knockouts, both in-frame deletions[16] and chromosomal losses[17] contribute to different expression profiles and clustering patterns of single cells.

Perhaps more interestingly, the heterogeneity perturbation responses may be driven by underlying biological factors (**Fig. 1a**). These factors may be either cell-intrinsic (e.g., the activities of other coding- and non-coding genomic elements) or cell-extrinsic (e.g., cell states or types, environment factors), all of which define the context of perturbation response. For example, combined expressions of transcription factors (TFs) are critical for many cellular state conversions. Therefore, to properly decode the functions of these TFs via perturbation, one must consider the effect of the cell state and the activities of other companion TFs. For this reason, defining the heterogeneity of perturbation response and identifying

factors that contribute to these outcomes is important for understanding how cells respond to perturbation.

Unfortunately, computational frameworks are currently lacking to decode the diverse outcomes of perturbations. For technical factors, mixscape is the only method to detect and mitigate confounding variations (e.g., incomplete knockouts from CRISPR/Cas9)[16]. However, its performance has not been rigorously benchmarked, especially when partial gene functions are perturbed using techniques like CRISPR interference (CRISPRi). More importantly, no methods have been developed to reveal new biological insights from the heterogenous perturbation outcomes, including studying how partial gene perturbations affect a phenotype of interest (i.e., "dosage" analysis), and discovering biological determinants that govern differential perturbation responses.

Here we present a computational framework, the perturbation-response score (PS), to quantify heterogenous perturbation outcomes in single-cell transcriptomics datasets. The PS, estimated from constrained quadratic optimization, quantifies the strength of the perturbation outcome for a single cell. We performed comprehensive benchmark studies that demonstrated the outstanding performance of PS over existing methods, including simulated datasets, genome-scale Perturb-seq, and published Perturb-seq datasets that cover various CRISPR-based technologies. More importantly, PS analysis presents two major conceptual advances for analyzing single-cell perturbation data: it enables analysis of the dose of perturbation, and identification of novel biological determinants that govern the heterogeneity of perturbation responses. First, we analyzed essential gene Perturb-seq and found two patterns of dose response, based on whether moderate perturbation leads to strong expression changes of downstream genes. Second, we identified intrinsic and extrinsic biological factors governing critical gene functions in latent HIV-1 expression and pancreatic/liver development. Based on PS analysis results, we identified and confirmed a novel function of CCDC6, wherein perturbation drives duodenum cell differentiation towards liver commitment. Collectively, PS analysis provides a powerful tool to decode heterogenous perturbation outcomes from single-cell assays.

Results

Using PS to detect heterogenous perturbation outcomes within and across datasets.

Perturbing the same gene (or non-coding elements) may result in different phenotypic changes or transcriptional outcomes (**Fig. 1a**), depending on technical factors (e.g., perturbation efficiency) and biological factors (e.g., cell type, cell state, activities of cofactors). Unfortunately, existing methods can detect only technical factors[16], while biological factors remain unexplored. To bridge this gap, we built a computational framework to quantify perturbation outcomes in single-cell datasets using scRNA-seq as readout. Corresponding assays include single-cell CRISPR screens (e.g., Perturb-seq), or simply multiplex scRNA-seq profiling of various perturbations (e.g., sci-Plex; **Fig. 1b, c**). We define the perturbation-response score (PS) to quantify the strength of perturbation, where PS=0 indicates no perturbation effect (e.g., effects corresponding to unperturbed, wild-type gene functions) and PS=1 indicates the maximum perturbation effect observed within a dataset; for example, effects that correspond to homozygous knockouts on both alleles of a gene. We utilize the expressions of multiple downstream targets of a perturbed gene to infer the (unknown) values of PS (**Fig. 1b**). For example, if one cell has dramatic expression changes on the known downstream target genes, then its value of PS should be higher than cells with weak expression changes of these genes.

We built a computational model, based on a constrained quadratic optimization, to automatically identify the downstream targets of perturbed genes and calculate PS (**Fig. 1c**). This model, named "scMAGeCK-PS", is based on our previously published scMAGeCK algorithm[15] and consists of three steps. First, scMAGeCK-PS identifies differentially expressed genes (DEGs) upon perturbation (e.g., perturbing the function of gene *X*), by comparing the transcriptome profiles between perturbed cells and unperturbed cells. These DEGs are served as "signature" target genes of *X*. Second, scMAGeCK-PS used a previously developed scMAGeCK model to estimate the average effect of perturbation on these target genes, which can be estimated from the first step. Third, scMAGeCK-PS uses a constraint optimization procedure to find the value of PS that minimizes the sum of mean squared errors between predicted and measured expression changes of all downstream targets (see Methods). The constraints are established such that any PS is non-negative for cells with *X* perturbed, and is exactly zero in cells without perturbation. Such constraints can be established based on the prior information of perturbations; for example, the expression matrix of single-guide RNAs (sgRNAs).

PS outperforms mixscape in quantifying partial perturbations.

mixscape[16] is currently the only method to detect and remove technical factors that affect perturbation outcomes, especially incomplete gene knockouts that are generated from CRISPR/Cas9. However, the performance of mixscape on partial gene perturbations has not been fully evaluated. Here we compare PS with mixscape using multiple benchmark datasets. We first used synthetic datasets to evaluate the performances of different methods, because finding a real scRNA-seq dataset that contains ground truth (*i.e.*, accurate measurements of loss-of-function upon perturbation) is challenging. For synthetic data generation, we used scDesign3[18] to simulate the single-cell transcriptomic responses upon perturbing the 50% and 100% functions of Nelfb, based on a real scRNA-seq dataset that deletes Nelfb in mouse T cells[19] (**Supplementary Fig. S1a;** see Methods). We specified different numbers of DEGs (from 10 to 500) and simulated their expression changes upon 50% or 100% perturbations of Nelfb functions. In all the cases, PS correctly estimated partial perturbation, where the median PSs range from 0.32-0.34 for 50% perturbation, and greater than 0.8 for 100% perturbation, respectively (**Fig. 1d-e; Supplementary Fig. S1b-e**). In contrast, mixscape uniformly assigned the posterior probability of perturbation to 1 in all cases, an indication that mixscape is not suited to analyze the outcome of partial gene perturbations (**Fig. 1d-e; Supplementary Fig. S1b-e)**, possibly due to the bimodal statistic model it uses, which only considers 100% knockout effects[16]**.**

We next evaluated different methods using real single-cell perturbation datasets. We chose CRISPRi-based Perturb-seq datasets (**Fig. 1f-i**) because the CRISPRi system directly modulates the expression levels of perturbed genes, and the perturbation efficiency can be accessed using single-cell transcriptomic data. We use two published K562 CROP-seq datasets:[20] in the first, only 1 gRNA is expressed within each cell (*i.e.,* low multiplicity of infection or MOI), and in the second multiple gRNAs are expressed (*i.e.,* high MOI). We examine cells where the transcription starting sites (TSS) of highly expressed protein-coding genes are targeted (23 and 342 genes, respectively; **Fig. 1g-i**, **Supplementary Fig. S1f-g**). If the TSS of gene *X* is perturbed, we first removed the expression of *X* from expression matrix, and used the rest of gene expressions to measure the perturbation efficiency of *X*. The scores of different methods were then compared with the expression of *X*, producing a direct measurement of perturbation efficiency (**Fig. 1f**). In over 40% of these genes (10 out of 23 for low MOI, 139 out of 342 for high MOI), PS has a strong negative correlation with the expression of *X* (**Fig. 1g**), defined as Pearson correlation coefficient < -0.1 and p value <0.01. In contrast, mixscape scores correlate with X expression in none of the genes (for low MOI dataset; **Fig. 1g),** or in less than 5% of all

173 the genes (for high MOI dataset; **Supplementary Fig. S1f-g**). PS detects a much greater number of cells
174 that have a strong perturbation effect (PS or mixscape score >0.5; **Fig. 1h**), whose scores are strongly
175 negatively correlated with gene expression (**Fig. 1i**). We also tested both methods in another CRISPRi-
176 based Perturb-seq dataset, where sgRNAs with mismatches reduce efficiency, leading to partial
177 perturbation effects[21] (**Supplementary Fig. S1h-i**). PS has a high sensitivity and a good balance
178 between sensitivity and specificity, evidenced by the higher Pearson correlation coefficients
179 (**Supplementary Fig. S1h**) and areas under the receiver-operating characteristic (ROC) curve (AUC)
180 values (**Supplementary Fig. S1i**).
181
182 To further benchmark methods in terms of a phenotype of interest, we designed and performed a
183 genome-scale CRISPRi Perturb-seq on both unstimulated and stimulated Jurkat, a T lymphocyte cell
184 model (**Fig. 2a**), and evaluated the performances of different methods in identifying known regulators of
185 T cell activation. We designed Perturb-seq library that contains sgRNAs targeting the TSS of 18,595
186 genes (4-6 guides per gene) and used a TAP-seq-based[22] multiplex primer panel to detect the
187 expressions of 374 genes with high sensitivity (see **Supplementary Table S1** and Methods). We
188 obtained high-quality scRNA-seq data on over 586,000 single cells after quality control, and the UMAP
189 clustering of Perturb-seq datasets clearly demonstrated the differences between stimulated and non-
190 stimulated cells (**Fig. 2b**). Next, we ran PS or mixscape to calculate the scores of all perturbations at a
191 single-cell level; and for each perturbed gene, we calculated its overall perturbation-response score, by
192 adding the scores of all cells that express a corresponding sgRNA targeting that gene. Because our
193 system focuses on T cell stimulation, perturbing a gene that reaches a highest (and lowest) cumulative
194 score should have the strongest (and no) effect on T cell stimulation, respectively. For an independent
195 evaluation, we extracted 385 (and 1297) positive (and negative) hits whose perturbation impairs (or does
196 not impair) the stimulation of T cells from a published genome-scale CRISPR screen[23]. Both Perturb-seq
197 and pooled CRISPR screen identified many known positive regulators of T cell activation, such as
198 components of the T cell receptor complex (e.g., CD3D) and proximal signaling components (e.g., LCK;
199 **Fig. 2c**). For many positive genes, cells with higher values of PS or mixscape score are skewed towards
200 non-stimulating state, consistent with their negative selections in pooled CRISPR screens using T cell
201 stimulation as readout (**Fig. 2c; Supplementary Fig. S2**). However, when comparing the ROC score,
202 PS reaches a higher AUC score than mixscape (**Fig. 2d**), indicating its better performance in accurately
203 separating positive from negative hits.
204
205 Finally, we tested different methods on a published ECCITE-seq, which simultaneously measures
206 single-cell transcriptomes, surface proteins, and perturbations[16]. PDL1 protein expression was used as an
207 independent metric of evaluation (**Fig. 2e**), because PDL1 is a well-studied gene whose protein
208 expression is well understood. Among 25 perturbed genes in the ECCITE-seq perturbation library, 17
209 are known to regulate PDL1 expression (**Fig. 2f**). We compared PS with mixscape in terms of predicting
210 changes in PDL1 expression (**Fig. 2f; Supplementary Fig. S3)**. In addition, the expression of the
211 perturbed gene is included in the comparison as a naïve method. In 19 out of 25 genes (76%), PS
212 outperformed mixscape and perturbed gene expression in predicting PDL1 expression (**Fig. 2e**),
213 including 12 out of 17 (71%) known PDL1 regulators. Notably, for genes whose perturbations led to
214 strong transcriptomic changes (*e.g.,* IFNGR1, IFNGR2, JAK2, STAT1), both PS and mixscape work
215 well, reaching AUC > 0.8 (**Fig. 2f**). For other genes whose perturbation only leads to moderate or weak
216 expression changes, as described previously[16], PS outperforms mixscape, including those that are
217 confirmed to be PLD1 regulators (*i.e.*, genes marked in red in **Fig. 2f**).
218

Analyzing dose-dependent effects of perturbation.

Traditionally, dosage analysis requires a careful, time-consuming adjustment of perturbation strength, including changing drug concentrations or designing sgRNA sequences to achieve various editing efficiencies[21,24]. Since the quantifying partial gene perturbation by PS is highly accurate (**Fig. 1-2**), we can use PS to perform dose-response analysis of perturbation, without the need to titrate the strength of perturbation. By examining ECCITE-seq data in which PDL1 expression was measured directly (**Fig. 2e**), we found correlations between PDL1 expression and the PS of known PDL1 regulators (**Fig. 3a**). The PSs of positive PDL1 regulators (e.g., IFNGR1/2, STAT1; **Fig. 3b**) are negatively correlated with PDL1 expression, while the scores of negative regulators (e.g., CUL3, BRD4) are negatively correlated (**Supplementary Fig. S3; Fig. 3c**). One example is CUL3, which is known to destabilize and degrade PDL1 protein expression[25]. Consequently, higher CUL3 PSs, indicating higher CUL3 functional perturbation, correspond to higher PDL1 protein expressions (**Fig. 3a**). Compared with mixscape, PS more accurately predicts the quantitative changes in PDL1 expression, evidenced by stronger Pearson correlations between the two (**Supplementary Fig. S3**).

We further investigated the relationships between perturbation efficiency and the strength of perturbation responses, which is measured by PS (**Fig. 3d**). In particular, we are interested in genes that show one of two different patterns of PSs upon perturbation: "buffered" distribution, where genes have high PSs only when stronger perturbation efficiency is achieved; and "sensitive" distribution, where the PSs are high, even with moderate or weak perturbation efficiency. Both "buffered" or "sensitive" terms have been coined previously to describe the effects of transcription factor dosages to chromatin accessibility[26]. CRISPRi-based Perturb-seq datasets are used, as the efficiencies of CRISPR inhibition can be directly evaluated by examining perturbed gene expressions (**Fig. 2e**).

We calculated PS for every gene in a published essential-wide Perturb-seq[27], which uses CRISPRi to inhibit the expressions of 2,285 common essential genes. We classified genes based on their PS quantiles that correspond to around 50% perturbation efficiency (**Fig. 3e**): a gene is classified as "buffered" if its median PS is smaller than 0.1; or "sensitive", if its 95% quantile is greater than 0.75. Among over 2,000 essential genes, we classified 613 genes as either buffered or sensitive. The majority are buffered (529 out of 613), indicating high robustness to perturbation, possibly due to their essential roles in cellular functions that require compensations on expression reductions. Many buffered genes belong to essential protein complexes, including proteosomes (e.g., PSMA3; **Fig. 3f**) and ribosomal subunits (e.g., RPL4; **Supplementary Fig. S4a**). 30% of the genes (185 out of 613) belong to "sensitive" category, showing strong transcriptome responses even with moderate or weak efficiencies upon perturbing gene expression (**Supplementary Fig. S4b-c**). Many of the sensitive genes are also displaying buffering effect, a demonstration of complex, heterogenous responses of cells undergoing the same perturbation of essential genes. Notably, 50% reduction of HSPA5 and GATA1 expression achieved near-maximal transcriptional response (and the associated growth defect), as in previous studies[22].

We further examined possible mechanisms by which buffered genes resist perturbation, especially those that belong to the same functional protein complex. Interestingly, perturbing one member of the protein complex usually leads to the expression up-regulation of other members of the complex, indicating a possible mechanism for compensation. For example, perturbing proteosome subunits led to a strong expression reduction of the perturbed gene (*e.g.,* PSMA5; blue squares in **Fig. 3g**) and concurrent up-regulation of other members of the proteosomes (*e.g.,* PSMB7, PSMD2). Perturbing many other protein

complexes, including ribosomal subunit, mediator, and RNA polymerases, also leads to similar up-regulation of some members of the same functional unit (**Supplementary Fig. S5a-c**), indicating that compensation occurs by up-regulation of other submits of the same molecular machine. To confirm our findings on a different cellular system, we examined the effects of perturbing proteosomes in our genome-scale Perturb-seq dataset (**Fig. 2a**). The TAP-seq approach used in this dataset provides a sensitive and accurate measurement of gene expression changes upon perturbation[27]. Indeed, perturbing members of the proteosome subunits leads to the up-regulation of other proteosomes (**Supplementary Fig. S5d**), consistent with the known transcriptional feedback loop that is observed between proteosome genes[28]. Overall, the widespread existence of such compensatory effect may explain the perturbation-expression phenotype of buffered genes, where a strong perturbation efficiency is needed to achieve strong expression changes.

PS reveals intrinsic and extrinsic biological factors that regulate gene functions in latent HIV expression.

We next perform Perturb-seq experiment and use PS to investigate the functions of key genes regulating latent HIV-1 expression. We used a Jurkat HIV cell model that we previously established for pooled CRISPR screening[29], where cells stably express Cas9 and are latently infected with HIV-GFP viral vector. We designed a Perturb-seq library that targets 10 protein-coding genes (**Supplementary Table S2**), which are either (1) known factors in HIV-1 virus expression and T cell activation (e.g., BIRC2), or (2) top hits from genome-scale CRISPR screens that we previously performed (e.g., BRD4)[29]. We performed Perturb-seq experiments in three different conditions, including stimulated Jurkat (by PMA/I) followed by GFP expression sorting (GFP+ or GFP-), and unstimulated cells (**Fig. 4a**). The single-cell transcriptomes were profiled via the 10X Genomics Chromium platform, and expressed guide RNAs can be captured directly. After quality controls, we received 7,063-8,811 single cells per sample, where the mean reads per cell (and median genes expressed per cell) in each sample is at least 69,888 (and 4,744), respectively (**Supplementary Fig. S6a**). Guide RNAs were detected in over 96% of the cells, and over 85% of these cells could be assigned a unique guide RNA (**Supplementary Table S3**). The transcriptome profiles of cells are primarily clustered by cell states (stimulated vs. unstimulated), indicating that the primary sources of expression variation are coming from cell states (**Fig. 4b**).

We investigated gene functions using our PS framework. Among all perturbed genes, the PS of BRD4 (bromodomain containing 4) demonstrates a strong cell state-specific pattern, where a subset of cells with BRD4 perturbation has strong BRD4 PSs (named "BRD4-PS+ cells") than other BRD4-perturbed cells (or "BRD4-PS- cells; **Fig. 4c**). BRD4-PS+ cells overexpress genes that are involved in known functions of BRD4[30,31] including NF-kB/TNF-alpha signaling, hypoxia and apoptosis (**Fig. 4c-d**, **Supplementary Fig. S6b-d**). We examined whether the differences in BRD4 PS reflects the degree of BRD4 functional perturbation. We first checked the expressions of BRD4 "signature" genes from another published study[32]. Compared with BRD4-PS- cells, BRD4-PS+ cells have a much lower expressions of these signature genes (**Supplementary Fig. S6e**), indicating a stronger functional BRD4 perturbation. In addition, BRD4 has been shown to inhibit HIV transcription and activation in many studies, including our previous CRISPR screens[29,33], consistent with the fact that HIV-GFP is one of the strongest up-regulated genes in BRD4-PS+ cells (**Supplementary Fig. S6f**). Furthermore, BRD4-PS+ cells have a stronger GFP expression (**Fig. 4d**) than other cells, confirming a stronger BRD4 functional perturbation in these cells.

310 To build a quantitative perturbation-expression relationship, we recalculated BRD4 PS without using
311 HIV-GFP expression and examined how the scores are associated with a phenotype of interest (i.e.,
312 latent HIV-GFP expression) in different conditions (**Fig. 4e**). BRD4 PS correlation with HIV-GFP
313 expression is cell-state dependent: in stimulated T cells (PMA/I treatment), a linear, positive correlation
314 is observed regardless of the GFP expression. In contrast, a nonlinear relationship exists in unstimulated
315 T cells (DMSO), where stronger BRD4 PS (>0.5) leads to a sharp increase in HIV-GFP expression (**Fig.**
316 **4e**).
317
318 Another gene, cyclin T1 (CCNT1), also displays heterogeneity in PS distribution: cells with CCNT1
319 perturbation have a high PS distribution only in stimulated cells (**Fig. 4f**). This is different from CCNT1
320 gene expression or guide distribution, which do not show such pattern differences between cell states
321 (**Supplementary Fig. S7a**). Confirming our findings, the number of DEGs (cells with CCNT1
322 perturbation vs. cells expressing non-targeting guides) is over 100 in stimulated cells, but only 1 in non-
323 stimulated cells (adjusted p value <0.001; **Supplementary Fig. S7b**). In particular, HIV-GFP is the
324 strongest DEG in cells with CCNT1 perturbation, consistent with the known role of CCNT1 in
325 activating HIV transcription.
326
327 CCNT1 is a key subunit of P-TEFb (positive transcription elongation factor b)/CDK9 complex that
328 drives RNA transcription, including the transcription of HIV. The transcription elongation control of P-
329 TEFb/CDK9 is a complicated process that is regulated by multiple mechanisms, including various T cell
330 signaling pathways (e.g., NF-kB signaling), translation control, and epigenetic modification (reviewed in
331 [34]). The activities of these factors are different in different states of T cells (e.g., NF-kB;
332 **Supplementary Fig. S7c**), which may explain the differences of CCNT1 PSs. Despite the strong cell
333 state dependency of CCNT1 PS, PS shows weak correlation with HIV-GFP within one cell state
334 (**Supplementary Fig. S7d**), which is different from BRD4 PS (**Fig. 4e**).
335
336 To further confirm our finding that different cellular states affect the transcriptomic responses of
337 CCNT1 perturbation, we stimulated Jurkat cells using a different agonist (TNF-alpha). To measure the
338 downstream effect of CCNT1 perturbation, we sorted cells by expression of HIV-GFP, which is the
339 strongest down-regulated gene upon CCNT1 knockout (**Supplementary Fig. S7b**), and whose
340 expression is known to be regulated by CCNT1[35,36]. Indeed, with the presence of TNF-alpha, CCNT1
341 knockout leads to a strong reduction in HIV-GFP expression (over 50% reduction), while such reduction
342 is much smaller (<5% reduction) in cellular states without TNF-alpha stimulation (**Fig. 4g**).
343 Collectively, these results demonstrated that PS is a powerful computational framework for investigating
344 cofactors (cell states, other genes) that drive transcriptomic responses upon gene perturbation.
345
346 **PS enables identification of novel cell-type dependent gene functions in regulating pancreatic cell**
347 **differentiation from multiplex single-cell transcriptomics.**
348 Besides Perturb-seq, multiplexing cells with different perturbations are also used to measure single-cell
349 responses to perturbation[2,19]. A mixture of cells from different perturbations can be sequenced at the
350 same time, and the identity of cells can be established using various methods including cell hashing[37],
351 the expressions of pre-defined barcodes[38], or a combination of random barcodes[39]. We therefore tested
352 our PS framework on pooled single-cell transcriptomics of different perturbations to study the functions
353 of lineage regulators during human pancreatic differentiation. By using an established in vitro human
354 embryonic stem cell (hESC) pancreatic differentiation system, we generated cells corresponding to early
355 stage (definitive endoderm, DE) and middle stage (pancreatic progenitor, PP) pancreas development. To

356 test the performance of PS framework and uncover the functions of unknown regulators, we picked ten
357 clonal hESC lines with the homozygous knockout of four genes (**Supplementary Table S4**), including
358 two known pancreatic lineage regulators (HHEX, FOXA1) and two uncharacterized candidate regulators
359 from previous genetic screens (OTUD5, CCDC6)[40,41]. These clones are then labelled with different
360 LARRY (Lineage and RNA recovery) DNA barcodes[38], pooled together and differentiated into DE and
361 PP stages using established protocols[40]. Finally, the single-cell expressions of these cells were profiled
362 via 10X genomics Chromium platform (**Fig. 5a**). The clone information of each cell was identified from
363 LARRY barcodes. Among 26,286 single cells that passed the quality control measurements, over 97%
364 (25,694/26,286) of the cells had at least one barcode detected, and over 80% (20,678/25,694) were
365 identified as singlets and retained for downstream analysis. UMAP clustering revealed different known
366 cell types during pancreatic differentiation, based on the expression markers of known cell types (**Fig.
367 5b; Supplementary Fig. S8**), including DE, PP, liver/duodenum progenitor (LV/DUO), endocrine
368 precursor (EP), and cells in transition stages (e.g., DE in transition, PP in transition).
369
370 We next applied the PS framework to the pooled single-cell RNA-seq datasets containing different
371 knockout clones. Among all knockout genes, HHEX PS is high in cells whose type is between two
372 different differentiated cell types (PP and LP/DP; **Fig. 5c; Supplementary Fig. S8**), consistent with the
373 known function of HHEX as a key determinant of cell fate decision, whose deletion drives DE cell
374 differentiation towards LP/DP, rather than PP[40]. Indeed, *HHEX* knockout led to a much fewer
375 percentage of cells that are annotated as PP (**Fig. 5d**). The PS of FOXA1, another key transcription
376 factor during PP differentiation, is strong in DE and PP cell types, consistent with the specific
377 expression pattern of FOXA1 in DE/PP cell types (**Supplementary Fig. S9a-c).**
378
379 As in our previous genome-wide CRISPR screens, CCDC6 is one of the top hits whose perturbation
380 hinders PP differentiation[40,42]. However, the exact function of CCDC6 during pancreatic differentiation
381 is largely unknown. CCDC6 may have different functions at different cell types, evidenced by the few
382 overlaps of DEGs between different cell types (**Supplementary Fig. S9d-f**). To investigate these
383 different functions, we calculated PSs from the DEGs from four major cell types in the dataset (DE in
384 transition, DE, PP/PP in transition, and LV/DUO). An unbiased clustering on these CCDC6 PSs
385 demonstrated two distinct distributions across cell types (**Fig. 5e**), where scores calculated from late-
386 stage cell types including PP/PP in transition/LV/DUO ("pattern 1") are distributed differently from
387 scores calculated from early-stage cell types including DE in transition/DE ("pattern 2"; **Fig. 5f;
388 Supplementary Fig. S10a-b**), implying different behaviors of CCDC6 perturbation at different cell
389 types. Indeed, functional analysis on DEGs leading to both patterns have distinct enrichment terms. In
390 early-stage cell types, DEG genes are enriched in the targets of stem cell transcription factors (e.g.,
391 SOX2, POU5F1, NANOG) and cell cycle regulation (**Supplementary Fig. S10c-e**), consistent with the
392 known function of *CCDC6* as a cell cycle regulator[43,44]. In contrast, DEGs in late-stage cell types are
393 primarily the targets of HNF4A, a key transcription factor that drives LP/DP differentiation (**Fig. 5g;
394 Supplementary Fig. S10f**). The expressions of these transcription factors (SOX2, HNF4A) are among
395 the up-regulated genes in both programs, respectively (**Supplementary Fig. S9d-e**). Furthermore,
396 compared with wild-type cells, *CCDC6* knockout cells have a much lower percentage of PP cells and a
397 higher percentage of LP/DP cells (**Fig. 5h**). Collectively, these results imply that *CCDC6* has different
398 functions for early vs. late-stage cell types. Especially in late-stage cell types, *CCDC6* knockout drives
399 cell differentiation towards LV/DUO cell types rather than PP cell types.
400

To further validate the prediction results of CCDC6, we performed flow cytometry analysis to evaluate the effects of *CCDC6* knockout on the composition of late-stage cell types (PP/LV/DUO). We examined the percentage of HNF4A+ cells, a marker for LV population, and PDX1+ cells, a marker for PP population. Indeed, both clones of *CCDC6* knockout greatly reduced PDX1+ population and increased HNF4A+ population in three biological replicates (**Fig. 5i; Supplementary Fig. S11**), confirming our finding on the enrichment of CCDC6 PS in LP/DP populations (**Fig. 5f-g**).

Discussion

Understanding cellular responses to perturbations is a central task in modern biology, from studying tumor heterogeneity to developing personalized medicine. These perturbations may be genetic (e.g., knocking out genes or non-coding elements), chemical (e.g., drug treatments), mechanical (e.g., pressure) or environmental (e.g., temperature changes). Single-cell genomics profiles of perturbations are commonly used to investigate the mechanisms of perturbations. Many technologies, including Perturb-seq and sci-Plex, provide a high-content readout of the results of systematically perturbing many genes or non-coding elements. Despite rapid technological advancements, a major bottleneck is the lack of a computational model to fully unlock the potential of high-content perturbation, especially for discovering novel biological insights from the data. Here we introduce the PS framework to model the heterogenous transcriptomic responses of perturbations and to enable novel biological discovery from modeling perturbation heterogeneity.

Partial gene perturbation is common in perturbation experiments. Partial perturbations may come from dose-controlled drug treatment, gene editing technology that does not fully knockout gene function (e.g., RNA- or CRISPR-interference, epigenome editors), or from CRISPR/Cas9 that generates random DNA editing outcomes. We demonstrated the outstanding performance of our PS method over existing methods in quantifying partial gene perturbation. Specifically, partial perturbation identification enables the analysis of dose-dependent effect, which is demonstrated in this study using various datasets.

More importantly, PS enables novel biological investigations, including analysis of perturbation dosage without the need to titrate perturbation strength and identification of cell-intrinsic and extrinsic biological factors that regulate perturbation responses. In the latter case, the PS, ranging between 0 and 1, no longer represents the quantity of partial perturbation, but instead represents the strength of the perturbation outcome. Therefore, PS becomes a convenient tool to identify cell context that determines perturbation outcome. We demonstrated the application of PS in various biological problems, including T cell activation, essential gene function, latent HIV-1 virus expression, and pancreatic cell differentiation. Importantly, our PS model leads the discovery of novel CCDC6 functions that are cell type dependent, whose role as a regulator during pancreatic and liver cell fate decision is experimentally validated.

Partial perturbations of gene functions contribute to the complexity of many biological processes. For example, “haploinsufficient” genes are able to cause disease phenotypes when 50% of their functions are disrupted, while “haplosufficient” genes will require a nearly complete gene knockout. However, we currently lack a method to investigate the phenotypes of partial gene perturbations or to efficiently perform dosage analysis at a large scale. Current approaches, such as introducing mismatches to guide RNAs to modulate the effects of CRISPRi[21] or Cas13[28], require a complex design of a specific CRISPR system. Here we demonstrated that both CRISPR knockout (e.g., **Fig. 2f, Fig. 4e**) and CRISPRi naturally introduce partial perturbation effects, which can be used to study the dose effect of partial gene

447 perturbations on downstream gene expressions or a phenotype of interest. Our PS framework is
448 versatile, enabling the dosage analysis using various perturbation methods (e.g., CRISPRi or CRISPR
449 knockout) and assays (e.g., Perturb-seq or multiplex scRNA-seq).
450
451 Results from genetic perturbations (e.g., via CRISPR/Cas9) are informative for drug development, and
452 confirmations from genetic perturbation experiments are usually required to demonstrate the feasibility
453 of candidate drug targets. However, titrating pharmaceutical interventions are easy (e.g., by using
454 different doses of drugs), while it is much more difficult to precisely control the degree of genetic
455 perturbations. Our PS framework provides a convenient alternative to dose-dependent perturbations,
456 especially genetic perturbations, and their associations with phenotypic changes, which will be
457 informative in designing drugs. For example, BRD4 is the primary target of bromodomain inhibitors
458 (BETi), many of which have been proposed as candidates of latency reversing agents (LRAs) to
459 reactivate latent HIV-1 expression. The distribution of BRD4 PSs (**Fig. 3**) reveals that stronger
460 perturbation effects are needed to induce the desired phenotype, in this case, the expression of HIV-GFP
461 (**Fig. 3**). Since BRD4 is an essential gene, a strong BRD4 perturbation may lead to unexpected toxicity,
462 thereby limiting the efficacy of BETi. Indeed, our previous study[29] demonstrated that 10-1000x higher
463 doses of JQ1, a commonly used BETi, are needed to induce latent HIV-1 expression at a similar level
464 with other potent LRAs. Our results further warrant the development of synergistic drug combinations to
465 mitigate the narrow therapeutic window of BETi, which is currently tested in many studies.
466
467 Our PS analysis provides a general framework to analyze several major sources that contribute to the
468 heterogeneity of perturbation responses: the strength of perturbation *per se* (e.g., **Fig. 1i, 3d;** BRD4 in
469 **Fig. 4c**), compensations to perturbation especially on essential genes (e.g., proteosomes; **Fig. 3g**), and
470 cell type/state specificity (e.g., T cell states in **Fig. 4**; differentiation cell types in **Fig. 5**). Importantly,
471 cell type/state is linked to perturbation responses in three distinct ways: cell type/state may change as a
472 result of perturbation (e.g., CCDC6 and HHEX in Fig. 5); cell type/state serving a critical context to
473 define perturbation responses (e.g., T cell states in response to CCNT1 perturbation in **Fig. 4f-g**); and
474 cell type/state as a confounding factor that drives perturbation responses (e.g., BRD4 perturbation
475 heterogeneity in unstimulated T cells in **Fig. 4c**). Compared with other methods, PS is currently the only
476 method to analyze heterogeneity of perturbation responses from all these aspects.
477
478 Confounding factors are the major sources of variation when analyzing single-cell perturbation effects.
479 These confounding factors can be modeled explicitly (e.g., using generalized linear models) if
480 confounding source is known; or be detected and corrected using mathematical or statistical approaches
481 including matrix factorization (e.g., using GSFA[45]) or independent component analysis (e.g., using
482 CINEMA-OT[46]). In contrast, PS does not explicitly model confounding factors. Instead, PS scores can
483 be used in combination with methods that remove confounding sources of variation, or to detect these
484 confounding factors that contribute to the heterogeneity in perturbation responses (e.g., **Fig. 4c**).
485 Importantly, many confounding factors defined in previous methods[16,46] are not always confounding;
486 instead, they can be used to discover novel biological insights, as are shown in this study (e.g.,
487 perturbation efficiency, cell type/state). The orthogonal algorithmic design of PS compared with existing
488 methods also allows the combination of PS with these methods to simultaneously remove confounding
489 factors and measure the strength of perturbation responses.
490
491 One limitation of PS is its power in detecting drastic changes in cell types or states. For example, even
492 moderate perturbations on essential gene functions affect cellular viability[47,48]. In this case, single-cell

profiling only captures surviving cells that are resistant to essential gene perturbations in various mechanisms (e.g., expression compensation in **Fig. 3**), and largely misses dead cells due to essential gene dysfunction. Consequently, due to this "survival bias", PS probably only reflects the perturbation responses in a fraction of cells, rather than the full spectrum of perturbations. To overcome this limitation, PS can combine with recently developed prediction methods that predict the responses of perturbations, even if cells between perturbed/non-perturbed states are unevenly distributed[49].

Methods

The Perturbation-response Score (PS) framework

Estimating PS proceeds in three steps, as illustrated in Figure 1c: target gene identification (Step 1), average perturbation effect estimation using a previously published scMAGeCK (Step 2), and PS estimation using constrained optimization (Step 3).

Step 1: target gene identification. We first performed differential expression analysis between cells with certain perturbation (e.g., knocking out gene *X*) and negative control cells. In most cases, negative control cells are cells that express non-targeting guide RNAs (in Perturb-seq), or wild-type cells (in pooled scRNA-seq). In Perturb-seq with high MOI condition, these cells may come from cells that do not have a particular perturbation. We used Wilcoxon rank sum test (implemented in Seurat) to identify and rank differentially expressed genes. Top genes were then selected as potential target genes of the specific perturbation. The maximum and minimum numbers of top genes can be specified by the user. Alternatively, users can provide the list of target genes for each perturbation, based on prior knowledge, therefore skipping the differential expression analysis in this step.

Step 2: average perturbation effect estimation. We used the linear regression module in scMAGeCK (scMAGeCK-LR) to estimate the average perturbation effect. scMAGeCK-LR takes the expressions of all target genes (identified in Step 1) in all cells as input and outputs a β score, which is conceptually similar to log fold change. There are two advantages of using β score, instead of simply using the log fold changes in Step 1. First, scMAGeCK-LR naturally supports datasets from high MOI Perturb-seq, where one cell may express multiple guides targeting different genes. Second, scMAGeCK-LR is able to estimate average perturbation effects of multiple perturbations (e.g., genome-scale perturbations) in one step, while a naïve DEG analysis can only calculate LFC for each perturbation.

The mathematical model of scMAGeCK-LR is described as follows. Let *Y* be the log-transformed, *M*N* expression matrix of *M* single cells and *N* target genes. These genes are the union of all target genes for all *K* perturbations, extracted from Step 1. Let *D* be the *M*K* binary cell identity matrix of *M* single cells and *K* perturbations, where $d_{jX} = 1$ if single cell *j* contains sgRNAs targeting gene *X* ($j = 1,2,\ldots,M; X = 1,2,\ldots,K$), and $d_{jX} = 0$ otherwise. *D* can be obtained from the detected guide RNA expression matrix from Perturb-seq or from the prior sample information from pooled scRNA-seq. The effect of target gene knockout on all expressed genes is indicated as a β score in a matrix B with size *K*N*, where $\beta_{XA} > 0$ (< 0) indicates gene *X* is positively (or negatively) selected on gene *A* expression, respectively. In other words, gene *X* knockout increases (or decreases) gene *A* expression if $\beta_{XA} > 0$ (< 0), respectively.

The log-transformed expression matrix *Y* is modeled as follows:

$$Y = Y_0 + D \times B + \epsilon, \qquad \text{Eq (1)}$$

where Y_0 is the basal expression level of all genes in an unperturbed state, and ϵ is a noise term following a Gaussian distribution with zero means. Y_0 can be estimated from negative control cells (e.g., wild-type cells or cells expressing non-targeting guides), or be modeled using the expressions of neighboring negative control cells (e.g., the approach used by mixscape[16]). The value of B can be estimated using ridge regression:

$$\mathrm{B} = (D^T D + \lambda I)^{-1} D^T Y, \qquad \text{Eq (2)}$$

where I is the identity matrix, and λ is a small positive value (default 0.01).

<u>Step 3: PS estimation using constrained optimization.</u> We revise Eq (1) to incorporate PS. Here, the log-transformed expression matrix Y is modelled as follows:

$$Y = Y_0 + \Psi \times B + \epsilon, \qquad \text{Eq (3)}$$

Where Ψ is the non-negative, raw PS matrix with the same size as D in Step 2 ($M*K$). Each element ψ_{jx} in Ψ indicates the raw PS of cell j of perturbing gene X. Here, B is the β score matrix which is estimated in Step 2. We find the value of Ψ to minimize the squared error of predicted and observed expressions of all genes within all cells, subject to constraints and regularization terms:

$$\min \sum_{ji} \left(y_{ji} - y_{ji}^0 - \sum_k \psi_{jk}\beta_{ki}\right)^2 + \lambda \sum_{jk} |\psi_{jk}|, \qquad \text{Eq (4)}$$

subject to the following constraints:

$$\begin{cases} 0 \le \psi_{jk} \le U, & if\ d_{jk} = 1 \\ \psi_{jk} = 0 & if\ d_{jk} = 0 \end{cases}.$$

Here, U is a positive value indicating the upper bound of raw Ψ values, and d_{ik} is the value of the binary cell identity matrix in Step 2. $1 \le j \le M$ is the index of single cells, $1 \le i \le N$ is the index of target genes, and $1 \le k \le K$ is the index of perturbations.

Because we are imposing non-negative constraints to Ψ, the absolute operator can be removed from the objective function in Eq (4) and can be rewritten as

$$\min \sum_{ji} \left(y_{ji} - y_{ji}^0 - \sum_k \psi_{jk}\beta_{ki}\right)^2 + \lambda \sum_{jk} \psi_{jk}\ . \qquad \text{Eq (4)}$$

This becomes a constrained quadratic optimization problem where the best solution can be easily achieved using methods like Newton's method. The final, normalized PS is to scale values of ψ_{ik} to [0,1]:

$$PS_{ik} = \psi_{ik}/U.$$

We implemented this framework as part of the scMAGeCK pipeline[18]. The PS source code, documentation and tutorials can be found on Github: https://github.com/davidliwei/PS

Simulated datasets

The eight simulated datasets are generated by the simulator scDesign3[46] with modifications for Perturb-seq. The simulation utilizes scDesign3's parametric model to capture the characteristics of the user-inputted reference data, specify the desired ground truth, and simulate synthetic cells via sampling from the model (to be detailed in **Steps 1-4** below). The reference data is the real scRNA-seq dataset with the gene Nelfb perturbed in some mouse T cells[47]; the cells with Nelfb perturbed are referred to as *knockout cells*, and the cells with Nelfb unperturbed serve as the negative control and are referred to as *wild-type cells*. Based on the same reference data, the eight simulated datasets are generated under eight different settings. Each setting corresponds to a combination of two simulation parameters' values: the number of Nelfb's downstream genes (i.e., the genes whose expression levels are affected by Nelfb's knockout; with candidate values 0, 10, 200, and 500) and the perturbation efficiency (with candidate values 50% and 100%). The candidate downstream genes of Nelfb are the top differentially expressed (DE) genes identified from the bulk RNA-seq data of the same biological sample (from the second sheet in the Excel file from Wu et al.'s Supplementary Data 1[48]). Thus, we have 4×2=8 simulated datasets in total.

Before running the simulation, we pre-process the scRNA-seq dataset and the bulk DE gene rank list.

1. First, we perform the same quality control as in the dataset's original publication[49]. Specifically, cells are retained only if their numbers of detected genes are between 1,000 and 5,000, and their UMI counts have less than 12% mitochondrial counts.
2. Second, we impute and amplify the gene-by-cell count matrix of the wild-type mouse cells to enhance the perturbation effects in the simulated data. Specifically, we first impute the wild-type count matrix using scImpute[50] (default version 0.0.9) to reduce the sparsity. Then we multiply the imputed count matrix by an amplification factor of 10 to increase the range of gene expression levels.
3. Third, we construct a gene-by-cell count matrix by combining the wild-type cells in the post-imputation-and-amplification wild-type count matrix and the knockout cells in the knockout count matrix. By the end of this step, the dimension of this combined matrix is $(P+1)\times N$, with rows corresponding to $P+1$ genes (Nelfb and P other genes) and columns corresponding to N cells, which consist of N^{wt} wild-type cells and N^{ko} knockout cells.
4. Fourth, we extract the row corresponding to Nelfb as a vector, which contains Nelfb's counts in all cells (an N-dimensional vector denoted as C, where C_j is Nelfb's count in cell j), and we denote the remaining P rows as a $P\times N$ matrix $\mathbf{Y}$, where Y_{ij} is gene i's count in cell j.
5. Fifth, using $\mathbf{Y}$, we refine the list of bulk DE genes by excluding the DE genes that correspond to zero rows in $\mathbf{Y}$ or do not correspond to any rows in $\mathbf{Y}$.
6. Lastly, to reduce the computation time for data simulation, we use the scran package[51] to select 3,000 highly variable genes in $\mathbf{Y}$. We only keep the union of these 3,000 highly variable genes and the refined bulk DE genes as the rows in $\mathbf{Y}$. The number of the kept genes is 3,390, so the dimension of $\mathbf{Y}$ is $3{,}390\times N$.

Additionally, we know which cells have Nelfb perturbed; thus, we have another N-dimensional binary vector denoted as K, where K_j indicates whether the j-th cell has Nelfb perturbed or not; that is, $K_j = 0$ means the j-th cell is a wild-type cell, and $K_j = 1$ means the j-th cell is a knockout cell. K and C are used as two covariate vectors, and $\mathbf{Y}$ is used as the reference count matrix for scDesign3. Finally, we modify scDesign3 by using $\mathbf{Y}$, C, K, the refined DE genes, the number of Nelfb's downstream genes, and the perturbation efficiency to simulate data in the following four steps:

Step 1: modeling each gene's marginal distribution independently. For each gene i, if it is a downstream gene of Nelfb, we assume that Y_{ij}, conditional on C_j, follows a zero-inflated negative binomial (ZINB) distribution with the mean parameter μ_{ij}, the dispersion parameter ϕ_i, and the zero-inflation probability parameter ν_{ij}. Otherwise, if gene i is not a downstream gene of Nelfb, we assume that Y_{ij} follows a ZINB distribution with the mean parameter μ_i, the dispersion parameter ϕ_i, and the zero-inflation probability parameter ν_i. This marginal distribution for each gene is specified by a generalized additive model for location, scale, and shape (GAMLSS). Without loss of generality, we define the first D genes in $\mathbf{Y}$ to be the top D DE genes in the refined DE gene list ($D \in \{0, 10, 200, 500\}$); we treat these top D DE genes as the D downstream genes of Nelfb. Then we modify scDesign3's original code implementation so Nelfb's downstream genes and non-downstream genes have different marginal distributions: a downstream gene's marginal distribution in each cell j depends on C_j, Nelfb's count in cell j; a non-downstream gene's marginal distribution in each cell j is irrelevant to C_j.

For Nelfb's downstream gene $i = 1, \dots, D$:

$$\begin{cases} Y_{ij} \mid C_j \sim \mathrm{ZINB}(\mu_{ij}, \phi_i, \nu_{ij}) \\ \log(\mu_{ij}) = \alpha_i + \beta_i \times C_j \\ \log(\phi_i) = \omega_i \\ \mathrm{logit}(\nu_{ij}) = \gamma_i + \eta_i \times C_j \end{cases}.$$

For Nelfb's non-downstream gene $i = D + 1, \dots, P$:

$$\begin{cases} Y_{ij} \sim \mathrm{ZINB}(\mu_i, \phi_i, \nu_i) \\ \log(\mu_i) = \alpha_i \\ \log(\phi_i) = \omega_i \\ \mathrm{logit}(\nu_i) = \gamma_i \end{cases}.$$

After parameter estimation by the R package gamlss, the fitted distribution of $Y_{ij} \mid C_j$, for $i = 1, \dots, D$, is denoted as $\mathrm{ZINB}(\hat{\mu}_{ij}, \hat{\phi}_i, \hat{\nu}_{ij})$ with the CDF $\hat{F}_{ij}$; the fitted distribution of Y_{ij}, for $i = D + 1, \dots, P$, is denoted as $\mathrm{ZINB}(\hat{\mu}_i, \hat{\phi}_i, \hat{\nu}_i)$ with the CDF $\hat{F}_i$. The other parameters including α_i, β_i, γ_i, and η_i are estimated as $\hat{\alpha}_i$, $\hat{\beta}_i$, $\hat{\gamma}_i$, and $\hat{\eta}_i$ for each i respectively.

Step 2: modeling genes' joint distribution using the Gaussian copula. To approximate the pairwise gene-gene correlations in the reference dataset, scDesign3 utilizes a multivariate statistical technique, the Gaussian copula. Given each gene's marginal distribution fitted in Step 1, scDesign3 approximates the multivariate joint distribution of the P genes in cell j as

$$\left(\Phi^{-1}(\hat{F}_{1j}(Y_{1j})), \dots, \Phi^{-1}(\hat{F}_{Dj}(Y_{Dj})), \Phi^{-1}(\hat{F}_{D+1}(Y_{(D+1)j})), \dots, \Phi^{-1}(\hat{F}_P(Y_{Pj}))\right) \sim N\left(\mathbf{0}, \hat{\mathbf{R}}(K_j)\right),$$

where $\Phi^{-1}(\cdot)$ denotes the inverse of the cumulative distribution function (CDF) of the standard Gaussian distribution, $\mathbf{0}$ is the P-dimensional zero vector, and $\hat{\mathbf{R}}(K_j)$ is the estimated $P \times P$ gene-gene correlation matrix of the Gaussian copula conditional on the value of K_j. Specifically, since K_j is binary, we have two estimated gene-gene correlation matrices, one for the wild-type cells ($K_j = 0$) and the other for the knockout cells ($K_j = 1$). For $\hat{F}_{1j}(Y_{1j}), \dots, \hat{F}_{Dj}(Y_{Dj}), \hat{F}_{D+1}(Y_{(D+1)j}), \dots, \hat{F}_P(Y_{Pj})$, a technique called "distributional transform" is used to make the CDFs continuous; see Sun et al.[52] for a detailed explanation.

Step 3: modifying the fitted parameters. Since we want to generate synthetic datasets with two perturbation efficiencies, for each downstream gene $i = 1, \dots, D$, we modify the mean parameters for all downstream genes in the knockout cells to reflect the user-specified perturbation efficiency. Without loss of generality, we assume the first $N^{\mathrm{ko}} = \sum_{j=1}^{N} I(K_j = 1)$ of the N cells as the knockout cells. Then, we update the mean parameters for Nelfb's D downstream genes in the N^{ko} knockout cells (i.e., $\hat{\mu}_{ij}$ for $i \in \{1, \dots, D\}$, $j \in \{1, \dots, N^{\mathrm{ko}}\}$) based on the user-specified perturbation efficiency as follows.

For the 50% perturbation efficiency: We randomly sample N^{ko} values from $\{C_j, j \in \{N^{\mathrm{ko}} + 1, \dots, N\}\}$ (i.e., Nelfb's counts in the wild-type cells) and multiply the sampled C_j values by 0.5 to represent the 50% perturbation efficiency. We store these sampled and scaled values by $C^* = \left(C_1^*, \dots, C_{N^{\mathrm{ko}}}^*\right)^T$ as Nelfb's counts in the N^{ko} synthetic knockout cells to be simulated. Then, we modify the mean parameters for the D downstream genes in the N^{ko} synthetic knockout cells (for $i \in \{1, \dots, D\}$, $j \in \{1, \dots, N^{\mathrm{ko}}\}$) as

$$\hat{\mu}_{ij} = \hat{\alpha}_i + \hat{\beta}_i \cdot C_j^* \ .$$

For the 100% perturbation efficiency: C^* becomes a zero vector with length N^{ko}, and we modify $\hat{\mu}_{ij}$ for $i \in \{1, \dots, D\}$, $j \in \{1, \dots, N^{\mathrm{ko}}\}$ in the same way as above.

We do not change any estimated mean parameters for the D downstream genes in the N^{wt} wild-type cells, any estimated mean parameters for the non-downstream $(P - D)$ genes in all N cells, any estimated dispersion parameters, or any estimated zero-inflation probability parameters.

Moreover, we use S to denote an N-dimensional vector representing Nelfb's counts in the N synthetic cells, with the counts in the first N^{ko} synthetic knockout cells set above based on the perturbation efficiency, and the counts in the last N^{wt} synthetic wild-type cells same as those in the real N^{wt} wild-type cells. That is, $S_j = C_j^*$ for $j \in \{1, \dots, N^{\mathrm{ko}}\}$, and $S_j = C_j$ for $j \in \{N^{\mathrm{ko}} + 1, \dots, N\}$.

Step 4: generating synthetic data with the fitted model and modified parameters. First, we independently sample N^{wt} Gaussian vectors of length P from the estimated P-dimensional multivariate Gaussian distribution $N\left(0, \widehat{\mathbf{R}}(K_j = 0)\right)$ and N^{ko} Gaussian vectors of length P from the estimated P-dimensional multivariate Gaussian distribution $N\left(0, \widehat{\mathbf{R}}(K_j = 1)\right)$. Together, we stack these $N = N^{\mathrm{wt}} + N^{\mathrm{ko}}$ vectors $(\tilde{Z}_{11}, \dots, \tilde{Z}_{P1})^T, \dots, (\tilde{Z}_{1N}, \dots, \tilde{Z}_{PN})^T$ by row into a $P \times N$ Gaussian matrix $\tilde{\mathbf{Z}}$.

Given the parameter estimates (modified or not) from Step 3, we convert the $P \times N$ Gaussian matrix $\tilde{\mathbf{Z}}$ into a $P \times N$ ZINB count matrix $\tilde{\mathbf{Y}}$ as

$$\tilde{\mathbf{Y}} = \begin{bmatrix} \tilde{Y}_1 = (\hat{F}_{11}{}^{-1}(\tilde{Z}_{11} | \hat{\mu}_{11}, \hat{\phi}_1, \hat{\upsilon}_{11}), \dots, \hat{F}_{1N}{}^{-1}(\tilde{Z}_{1N} | \hat{\mu}_{1N}, \hat{\phi}_1, \hat{\upsilon}_{1N})) \\ \vdots \\ \tilde{Y}_D = (\hat{F}_D{}^{-1}(\tilde{Z}_{D1} | \hat{\mu}_{D1}, \hat{\phi}_D, \hat{\upsilon}_{D1}), \dots, \hat{F}_{DN}{}^{-1}(\tilde{Z}_{DN} | \hat{\mu}_{DN}, \hat{\phi}_D, \hat{\upsilon}_{DN})) \\ \tilde{Y}_{D+1} = (\hat{F}_{D+1}{}^{-1}(\tilde{Z}_{(D+1)1} | \hat{\mu}_{D+1}, \hat{\phi}_{D+1}, \hat{\upsilon}_{D+1}), \dots, \hat{F}_{D+1}{}^{-1}(\tilde{Z}_{(D+1)N} | \hat{\mu}_{D+1}, \hat{\phi}_{D+1}, \hat{\upsilon}_{D+1})) \\ \vdots \\ \tilde{Y}_P = (\hat{F}_P{}^{-1}(\tilde{Z}_{P1} | \hat{\mu}_P, \hat{\phi}_P, \hat{\upsilon}_P), \dots, \hat{F}_P{}^{-1}(\tilde{Z}_{PN} | \hat{\mu}_P, \hat{\phi}_P, \hat{\upsilon}_P)) \end{bmatrix}.$$

Lastly, we combine $\widetilde{\mathbf{Y}}$ with S by row into a $(P+1)\times N$ matrix, obtaining the final $(P+1)\times N$ synthetic count matrix ($\begin{bmatrix}\widetilde{\mathbf{Y}}\\ S\end{bmatrix}$).

Genome-scale Perturb-seq on Jurkat cells

Perturb-seq. We performed genome-scale Perturb-seq on Jurkat E6 cell line expressing dCas9-KRAB as our model to study. We transduced them with a genome-wide CRISPRi CROP-seq library at a high MOI. After infection, we split the cells into two populations, including untreated cells and activated cells (cells treated with anti-TCR and anti-CD28 antibodies for approximately 24 hours to stimulate TCR signaling). Cells were then labelled with cell hashing antibodies. Multiple labels were used for the activated population to help with cell multiplet detection. Cells were loaded on 16 channels of a 10x Chromium X instrument. We loaded 115 000 cells per channel, and the expected recovery rate was 60 000 cells per channel, including 24% multiples. Samples were pooled unequally before they were loaded on the ChromiumX: 10% untreated cells, 90% treated cells. A sequencing library was prepared using 3'Chemistry with a targeted primer panel: custom multiplex PCR step to enrich for specific transcripts. Libraries were sequenced on NovaSeq S4 PE100 in asymetric read mode (R1: 28 cycles; R2: 172 cycles), with PhiX concentration of 1%. The expected coverage is around 9 000 ~ 10 000 input reads per cell.

Hash oligos.

oligo	condition
CGGCTCGTGCTGCGTCGTCTCAAGTCCAGAAACTCCGTGTATCCT	untreated
CTCCCTGGTGTTCAATACCCGATGTGGTGGGCAGAATGTGGCTGG	activated
TTACCCGCAGGAAGACGTATACCCCTCGTGCCAGGCGACCAATGC	activated
TGTCTACGTCGGACCGCAAGAAGTGAGTCAGAGGCTGCACGCTGT	activated
CCCCACCAGGTTGCTTTGTCGGACGAGCCCGCACAGCGCTAGGAT	activated
GTGATCCGCGCAGGCACACATACCGACTCAGATGGGTTGTCCAGG	activated
GCAGCCGGCGTCGTACGAGGCACAGCGGAGACTAGATGAGGCCCC	activated

sgRNA library design. The genome-wide CRISPRi sgRNA library was designed to target the transcription start site (TSS) coordinates, calculated from publicly available FANTOM CAGE peaks data. In total, 18 595 genes were targeted, with 4 sgRNAs per gene. On top of that, we designed another CRISPRi library targeting 3220 genes with 4 sgRNAs per gene. This library was designed using Jurkat-specific TSS, which were calculated from public Jurkat CAGE-seq datasets. Both libraries were combined into a final library targeting 3220 genes with 8 sgRNA/gene and 15 375 genes with 4 sgRNA/gene.

Targeted primer panel. The primer panel for targeted transcriptomic readout consisted of 374 target genes from several categories:

Source	Number of targets (genes)
bulk RNA-seq DEG, 50 top up/downregulated	100
T-cell related genes	51
KEGG TCR signaling pathway	35
RNA-binding proteins	27

Replogle*: unfolded protein response	51
Replogle: proteasome	41
Replogle: NFkB	20
Replogle: cell cycle	29
Replogle: targets of nonsense-mediated decay	5
Controls (cell cycle, mitochondrial, Cas9)	15
Total number of targets	374

732
733 * "Replogle" prefix means that this category of targets was derived from the published genome-scale
734 Perturb-seq dataset[50].
735
736 Data preprocessing. For each of the 16 channels, all 3 kinds of sequencing libraries (mRNA, sgRNA,
737 cell hashing) were indexed using the same Illumina index sequence. We obtained high-quality scRNA-
738 seq data of over 586,000 single cells after quality control, with a median 13 guides detected per cell. We
739 obtained an average of 400 cells per gene perturbation. STAR and STAR solo 2.7.10a were used to map
740 transcriptomic reads against a custom gtf annotation, which was based on gencode.v34.annotation.gtf
741 (hg38). Reads that did not map to the transcriptome reference were then mapped & counted using STAR
742 solo against a custom fasta reference with guide sequences and a fasta reference with hash label
743 sequences. STAR Solo output transcriptome matrices were first filtered using an approach similar to 10x
744 cellranger EmptyDrops filtering, which retained cells with at least 10 % UMI count of the 99th percentile
745 UMI counts of the top expected cells number. Then, an initial Seurat object was created from those
746 filtered transcriptome matrices using the CreateSeuratObject function with following parameters:
747 min.cells = 5; min.features = 10; all other parameters at default values. Outlier cells were filtered out by
748 mithochondrial and mRNA content (percent.mt, nCount_RNA). In order to detect cell multiplets and
749 determine cell population (untreated or activated), cell labels (also known as hashes) were called using
750 the MULTI-seq approach (deMULTIplex::classifyCells in R). Only cells with exactly 1 known label
751 were kept. Then, sgRNA calling was conducted using a binomial test, with total sgRNA UMI counts
752 used to derive background frequencies. A threshold of 0.05 on Benjamini-Hochberg corrected p-values
753 (per channel) was use to generate the final calls. The sgRNA assays are sparse matrices containing 1,
754 where the respective cell is considered to be carrying the respective sgRNA and 0 elsewhere. Following
755 that, all results from steps above from 16 channels were merged together, and merged counts were
756 normalized using NormalizeData and scaled using ScaleData. Cell cycle scoring was performed via
757 CellCycleScoring, PCA was calculated using RunPCA, and UMAP was calculated on first 30 principal
758 components using RunUMAP in Seurat.
759
760 **HIV latency Perturb-seq**
761 We used a previously established cell line model of HIV latency[40]. In this model, Jurkat cells were
762 infected with an HIV vector with GFP tied to the LTR promoter, resulting in a positive GFP signal as a
763 measurement of viral transcription reactivation and HIV latency reversal. These cells, which already
764 express Cas9, were transduced with a lenti-sgRNA library. The lenti-sgRNA library (MilliporeSigma;
765 LV14, U6-gRNA-10x:EF1a-Puro-2a-BFP) was designed to target 10 genes, with 3 gRNAs per gene. In
766 addition to non-targeting controls, the library contained five positive regulators (NFKB1, CCNT1,
767 PRKCA, TLR1, MAP3K14) and five negative regulators (NFKBIA, NELFE, HDAC2, BRD4, BIRC2)
768 of HIV transcription. Transduction was carried out on 850,000 cells at an MOI of 0.3 using 8ug/ml
769 polybrene in 2 ml of RPMI containing 10% FBS and 1% penicillin–streptomycin. The media was
770 replaced 24 hours later with fresh media without polybrene. Two days after transduction, the cells were

771 selected for using 1.5 ug/ml puromycin for 5 days. After selection, the cells were split evenly into three
772 groups. One-third of the cells were kept in culture with no drug added, and two-thirds of the cells were
773 stimulated with PMA/I (50ng/ml PMA in combination with 1 μM Ionomycin). After 16 hours, the
774 stimulated cells were sorted into GFP+ and GFP- populations. All three samples were then analyzed
775 following the 10x Genomics single-cell sequencing protocol. Sequencing data, encompassing gene
776 expression and CRISPR guide capture libraries, underwent demultiplexing and processing using Cell
777 Ranger (version 6.1.2). The resulting feature-barcode matrices from three samples were then merged,
778 and subsequent analysis was carried out utilizing the Seurat R package (version 4.3.1). To ensure data
779 quality, cells were excluded if the number of expressed genes was greater than 7,500 or fewer than 200.
780 Additionally, cells were removed if the percentage of mitochondrial reads exceeded 15%. Single cells
781 harboring more than one detected sgRNA sequence, attributable to either multiple sgRNA transductions
782 or the presence of multiple cells in a single-cell droplet, were also excluded from the analysis. Following
783 quality control measures, merged counts underwent normalization and scaling. PCA was computed
784 based on the top 2,000 highly variable genes. Subsequently, clustering and UMAP embeddings were
785 performed using default parameters. To gain further insights into the biological significance of the
786 obtained clusters, enrichment analysis was conducted utilizing Enrichr (PMID: 27141961).
787
788 **Pancreatic differentiation clones and pooled single-cell RNA-seq**
789 Culture of hESC. Generation of KO hESCs was described in published studies, including HHEX KO H1
790 and HUES8 cell lines[53], FOXA1 KO HUES8 cell lines[54], OTUD5 KO HUES8 cell lines, and CCDC6
791 KO H1 cell lines[41]. Cells were regularly confirmed to be mycoplasma-free by the Memorial Sloan
792 Kettering Cancer Center (MSKCC) Antibody & Bioresource Core Facility. KO and WT hESCs were
793 maintained in Essential 8 (E8) medium (Thermo Fisher Scientific, A1517001) on vitronectin (Thermo
794 Fisher Scientific, A14700) pre-coated plates at 37 °C with 5% CO2. The Rho-associated protein kinase
795 (ROCK) inhibitor Y-276325 (5 μM; Selleck Chemicals, S1049) was added to the E8 medium the first
796 day after passaging or thawing of hESCs.
797
798 hESC-directed pancreatic differentiation. hESCs were seeded at a density of 2.3×10^5 cells/cm^2 on
799 vitronectin-coated plates in E8 medium with 10 μM Y-27632. After 24 hours, cells were washed with
800 PBS and differentiated to DE (stage 1), primitive gut tube (stage 2), PP1 (stage 3) and PP2 (stage 4)
801 stages following previously described 4-stage protocol[40]. In brief, stage 1 (3 d): S1/2 medium
802 supplemented with 100 ng ml^{-1} Activin A (Bon Opus Biosciences) and 5 μM CHIR99021 (04-0004-10,
803 Stemgent) for 1 d. S1/2 medium supplemented with 100 ng ml^{-1}Activin A for the next 2 d. Stage 2 (2 d):
804 S1/2 medium supplemented with 50 ng ml^{-1} KGF (AF-100-19, PeproTech) and 0.25 mM vitamin C
805 (VitC) (Sigma-Aldrich, A4544). Stage 3 (2 d): S3/4 medium supplemented with 50 ng ml^{-1} KGF,
806 0.25 mM VitC and 1 μM retinoic acid (R2625, MilliporeSigma). Stage 4 (4 d): S3/4 medium
807 supplemented with 50 ng ml^{-1} KGF, 0.1 μM retinoic acid, 200 nM LDN (Stemgent, 04-0019), 0.25 μM
808 SANT-1 (Sigma, S4572), 0.25 mM VitC and 200 nM TPB (EMD Millipore, 565740). The base
809 differentiation medium formulations used in each stage were as follows. S1/2 medium: 500 ml MCDB
810 131 (15-100-CV, Cellgro) supplemented with 2 ml 45% glucose (G7528, MilliporeSigma), 0.75 g
811 sodium bicarbonate (S5761, MilliporeSigma), 2.5 g BSA (68700, Proliant), 5 ml GlutaMAX (35050079,
812 Invitrogen). S3/4 medium: 500 ml MCDB 131 supplemented with 0.52 ml 45% glucose, 0.875 g sodium
813 bicarbonate, 10 g BSA, 2.5 ml ITS-X, 5 ml GlutaMAX.
814
815 Cell infection with LARRY barcode virus. Individual LARRY barcode constructs were cloned from the
816 LARRY barcode library (Addgene:140024) and transfected to 293T cells to generate lentivirus. Next,

each KO and WT hESC clone was infected with a unique LARRY barcode at low MOI. One week after lentiviral infection, the barcoded cells, which expressed GFP, were sorted out and cultured in E8 medium as described in previous section.

Pooled single-cell RNA-seq. One day before differentiation, each of 10 hESC barcoded clones were counted, mixed at the same cell number ratio, and then seeded at a density of 2.3×10^5 cells/cm^2 onto a 12-well cell culture plate. At DE and PP2 stages, pooled differentiating cells were dissociated into single cell suspension by TrypLE Select for 5 min at 37 °C. Cells were then stored in BAMBANKER™ freezing medium for future experiments. For scRNA-seq, frozen cells were thawed and sorted to collect live GFP+ cells. Cellular suspensions were then loaded on a Chromium Controller following the manufacturer's instructions (10x Genomics Chromium Single Cell 3′ Reagent Kit v3.1 User Guide). cDNA libraries and targeted LARRY barcode libraries were generated separately using 10ul cDNA each. cDNA libraries were made under manufacturer's instructions and targeted LARRY barcode libraries were amplified using specific primers (F: CTACACGACGCTCTTCCGATCT; R: GTGACTGGAGTTCAGACGTGTGCTCTTCCGATCTtaaccgttgctaggagagaccataT).

Data analysis. The sequencing data which included transcriptome and LARRY barcode libraries, underwent demultiplexing and processing via Cell Ranger (version 6.1.2). Subsequent analysis was conducted using the Seurat R package (version 4.3.1). Quality control measures were implemented to ensure robust data analysis. Cells were excluded if the number of expressed genes exceeded 7,000 or fell below 200. Additionally, cells were removed if the percentage of mitochondrial read exceeded 20%. Singlet cells were defined by considering the highest feature barcode count, ensuring it was at least twice as large as the second highest feature barcode count. Single cells containing more than one detected barcode sequence were excluded from the dataset. This process resulted in a final set of 20,678 cells for downstream analysis. After quality control measures, the count matrix underwent normalization and scaling. PCA was performed using the top 2,000 highly variable genes. Subsequently, clustering and UMAP embeddings were generated using default parameters to elucidate the underlying structure and relationships within the dataset.

Flow cytometry. Cells were dissociated using TrypLE Select and resuspended in FACS buffer (5% FBS in PBS). Live/Dead Fixable Violet cell stain (Invitrogen, L34955) was used to discriminate dead cells from live cells. Permeabilization/fixation was performed at room temperature for 1 h. Antibody staining was performed in permeabilization buffer. Antibodies for this study include HNF4A, Novus Biologicals, NBP2-67679, 1:200; PDX1, R&D Systems, AF2419, 1:500, Donkey anti-Rabbit IgG (H+L) Highly Cross-Adsorbed Secondary Antibody, Thermo Fisher Scientific, 1:500; Donkey anti-goat IgG (H+L) Highly Cross-Adsorbed Secondary Antibody, Thermo Fisher Scientific, 1:500. Cells were then analysed using BD LSRFortessa. Flow cytometry analysis and figures were generated using FlowJo v.10.

Acknowledgements

The authors thank all members from the Li and Huangfu laboratory for comments and discussions. The authors thank Jake P. Taylor-King for discussions. This study is supported by NIH R01 HG010753, HL168174 (to W.L., B.S., L.C.), District of Columbia Center for AIDS (DC-CFAR) Research Transitioning Investigator Award (AI117970, to W.L.), and startup support from the Center for Genetic Medicine Research at Children's National Hospital. D.H is supported by NIH UM1 HG012654, U01 HG012051. J.J. Li is supported by National Science Foundation DBI-1846216 and DMS-2113754, NIH R35 GM140888, Johnson and Johnson WiSTEM2D Award, Sloan Research Fellowship, UCLA David

Geffen School of Medicine W.M. Keck Foundation Junior Faculty Award, and Chan-Zuckerberg Initiative Single-Cell Biology Data Insights [Silicon Valley Community Foundation Grant Number: 2022-249355]. W.D. and R.F.S. is supported by the Howard Hughes Medical Institute.

Author contributions

W.L. conceived the project. W.L. and B.S. developed the method. W.L., B.S., and D.L. designed and performed the experiments and analyzed the data. W.D., N.M. and B.S. performed and analyzed HIV Perturb-seq under the supervision of J.M.S., R.S. and W.L. B.S., Q.W. and D.S. performed synthetic experiments under the supervision of W.L. and J.J.L. D.L., D.Y., B.W. and B.R. generated pancreatic differentiation dataset and performed validations under the supervision of D.H. A.K., A.V., N.U., and A.L. generated and analyzed genome-scale Perturb-seq under the supervision of T.B. X.C., L.C. and Y.D. performed the analysis and interpretation of the results. W.L., and B.S. wrote the manuscript with input from all the authors. W.L. T.B., J.J.L., R.S. and D.H. supervised the study.

Competing interests

T.B. is a co-founder and Managing Director of Myllia Biotechnology. A.K., A.V., N.U. and A.L. are employees of Myllia Biotechnology. Other authors declare that they have no competing interest.

Data and materials availability

The Perturb-seq scRNA-seq data have been deposited to Gene Expression Omnibus (GEO) under the accession number GSE247601. The source code of the PS method, and the documentation and demos are available on GitHub: (https://github.com/davidliwei/PS).

References

1 High-content CRISPR screening. *Nat Rev Methods Primers* 2022;**2**:. https://doi.org/10.1038/s43586-022-00098-7.

2 Srivatsan SR, McFaline-Figueroa JL, Ramani V, Saunders L, Cao J, Packer J, *et al.* Massively multiplex chemical transcriptomics at single-cell resolution. *Science* 2020;**367**:45–51.

3 Dixit A, Parnas O, Li B, Chen J, Fulco CP, Jerby-Arnon L, *et al.* Perturb-Seq: Dissecting Molecular Circuits with Scalable Single-Cell RNA Profiling of Pooled Genetic Screens. *Cell* 2016;**167**:1853-1866.e17.

4 Adamson B, Norman TM, Jost M, Cho MY, Nuñez JK, Chen Y, *et al.* A Multiplexed Single-Cell CRISPR Screening Platform Enables Systematic Dissection of the Unfolded Protein Response. *Cell* 2016;**167**:1867-1882.e21.

5 Jaitin DA, Weiner A, Yofe I, Lara-Astiaso D, Keren-Shaul H, David E, *et al.* Dissecting Immune Circuits by Linking CRISPR-Pooled Screens with Single-Cell RNA-Seq. *Cell* 2016;**167**:1883-1896.e15.

6 Datlinger P, Rendeiro AF, Schmidl C, Krausgruber T, Traxler P, Klughammer J, *et al.* Pooled CRISPR screening with single-cell transcriptome readout. *Nat Methods* 2017;**14**:297–301.

908 7 Xie S, Duan J, Li B, Zhou P, Hon GC. Multiplexed Engineering and Analysis of Combinatorial
909 Enhancer Activity in Single Cells. *Mol Cell* 2017;**66**:285-299.e5.
910 8 Rubin AJ, Parker KR, Satpathy AT, Qi Y, Wu B, Ong AJ, *et al.* Coupled Single-Cell CRISPR
911 Screening and Epigenomic Profiling Reveals Causal Gene Regulatory Networks. *Cell*
912 2019;**176**:361-376.e17.
913 9 Liscovitch-Brauer N, Montalbano A, Deng J, Méndez-Mancilla A, Wessels H-H, Moss NG, *et al.*
914 Profiling the genetic determinants of chromatin accessibility with scalable single-cell CRISPR
915 screens. *Nat Biotechnol* 2021;**39**:1270–7.
916 10 Dhainaut M, Rose SA, Akturk G, Wroblewska A, Nielsen SR, Park ES, *et al.* Spatial CRISPR
917 genomics identifies regulators of the tumor microenvironment. *Cell* 2022;**185**:1223-1239.e20.
918 11 Norman TM, Horlbeck MA, Replogle JM, Ge AY, Xu A, Jost M, *et al.* Exploring genetic
919 interaction manifolds constructed from rich single-cell phenotypes. *Science* 2019;**365**:786–93.
920 12 Replogle JM, Norman TM, Xu A, Hussmann JA, Chen J, Cogan JZ, *et al.* Combinatorial single-cell
921 CRISPR screens by direct guide RNA capture and targeted sequencing. *Nat Biotechnol*
922 2020;**38**:954–61.
923 13 Wessels H-H, Méndez-Mancilla A, Hao Y, Papalexi E, Mauck WM 3rd, Lu L, *et al.* Efficient
924 combinatorial targeting of RNA transcripts in single cells with Cas13 RNA Perturb-seq. *Nat*
925 *Methods* 2023;**20**:86–94.
926 14 Hill AJ, McFaline-Figueroa JL, Starita LM, Gasperini MJ, Matreyek KA, Packer J, *et al.* On the
927 design of CRISPR-based single-cell molecular screens. *Nat Methods* 2018;**15**:271–4.
928 15 Yang L, Zhu Y, Yu H, Cheng X, Chen S, Chu Y, *et al.* scMAGeCK links genotypes with multiple
929 phenotypes in single-cell CRISPR screens. *Genome Biol* 2020;**21**:19.
930 16 Papalexi E, Mimitou EP, Butler AW, Foster S, Bracken B, Mauck WM 3rd, *et al.* Characterizing
931 the molecular regulation of inhibitory immune checkpoints with multimodal single-cell screens.
932 *Nat Genet* 2021;**53**:322–31.
933 17 Tsuchida CA, Brandes N, Bueno R, Trinidad M, Mazumder T, Yu B, *et al.* Mitigation of
934 chromosome loss in clinical CRISPR-Cas9-engineered T cells. *Cell* 2023;**186**:4567-4582.e20.
935 18 Song D, Wang Q, Yan G, Liu T, Sun T, Li JJ. scDesign3 generates realistic in silico data for
936 multimodal single-cell and spatial omics. *Nat Biotechnol* 2023. https://doi.org/10.1038/s41587-023-
937 01772-1.
938 19 Wu B, Zhang X, Chiang H-C, Pan H, Yuan B, Mitra P, *et al.* RNA polymerase II pausing factor
939 NELF in CD8+ T cells promotes antitumor immunity. *Nat Commun* 2022;**13**:2155.
940 20 Gasperini M, Hill AJ, McFaline-Figueroa JL, Martin B, Kim S, Zhang MD, *et al.* A Genome-wide
941 Framework for Mapping Gene Regulation via Cellular Genetic Screens. *Cell* 2019;**176**:1516.
942 21 Jost M, Santos DA, Saunders RA, Horlbeck MA, Hawkins JS, Scaria SM, *et al.* Titrating gene
943 expression using libraries of systematically attenuated CRISPR guide RNAs. *Nat Biotechnol*
944 2020;**38**:355–64.
945 22 Schraivogel D, Gschwind AR, Milbank JH, Leonce DR, Jakob P, Mathur L, *et al.* Targeted
946 Perturb-seq enables genome-scale genetic screens in single cells. *Nat Methods* 2020;**17**:629–35.
947 23 Shifrut E, Carnevale J, Tobin V, Roth TL, Woo JM, Bui CT, *et al.* Genome-wide CRISPR screens
948 in primary human T cells reveal key regulators of immune function. *Cell* 2018;**175**:1958-1971.e15.
949 24 Wessels H-H, Stirn A, Méndez-Mancilla A, Kim EJ, Hart SK, Knowles DA, *et al.* Prediction of on-
950 target and off-target activity of CRISPR-Cas13d guide RNAs using deep learning. *Nat Biotechnol*
951 2023. https://doi.org/10.1038/s41587-023-01830-8.
952 25 Zhang J, Bu X, Wang H, Zhu Y, Geng Y, Nihira NT, *et al.* Cyclin D–CDK4 kinase destabilizes
953 PD-L1 via cullin 3–SPOP to control cancer immune surveillance. *Nature* 2018;**553**:91–5.

954 26 Naqvi S, Kim S, Hoskens H, Matthews HS, Spritz RA, Klein OD, *et al.* Precise modulation of
955 transcription factor levels identifies features underlying dosage sensitivity. *Nat Genet* 2023;**55**:841–
956 51.
957 27 Replogle JM, Saunders RA, Pogson AN, Hussmann JA, Lenail A, Guna A, *et al.* Mapping
958 information-rich genotype-phenotype landscapes with genome-scale Perturb-seq. *Cell*
959 2022;**185**:2559-2575.e28.
960 28 Radhakrishnan SK, Lee CS, Young P, Beskow A, Chan JY, Deshaies RJ. Transcription factor Nrf1
961 mediates the proteasome recovery pathway after proteasome inhibition in mammalian cells. *Mol*
962 *Cell* 2010;**38**:17–28.
963 29 Dai W, Wu F, McMyn N, Song B, Walker-Sperling VE, Varriale J, *et al.* Genome-wide CRISPR
964 screens identify combinations of candidate latency reversing agents for targeting the latent HIV-1
965 reservoir. *Sci Transl Med* 2022;**14**:eabh3351.
966 30 Yin M, Guo Y, Hu R, Cai WL, Li Y, Pei S, *et al.* Potent BRD4 inhibitor suppresses cancer cell-
967 macrophage interaction. *Nat Commun* 2020;**11**:1833.
968 31 Tan Y-F, Wang M, Chen Z-Y, Wang L, Liu X-H. Inhibition of BRD4 prevents proliferation and
969 epithelial-mesenchymal transition in renal cell carcinoma via NLRP3 inflammasome-induced
970 pyroptosis. *Cell Death Dis* 2020;**11**:239.
971 32 Shu S, Wu H-J, Ge JY, Zeid R, Harris IS, Jovanović B, *et al.* Synthetic Lethal and Resistance
972 Interactions with BET Bromodomain Inhibitors in Triple-Negative Breast Cancer. *Mol Cell*
973 2020;**78**:1096-1113.e8.
974 33 Li Z, Guo J, Wu Y, Zhou Q. The BET bromodomain inhibitor JQ1 activates HIV latency through
975 antagonizing Brd4 inhibition of Tat-transactivation. *Nucleic Acids Res* 2013;**41**:277–87.
976 34 Mbonye U, Kizito F, Karn J. New insights into transcription elongation control of HIV-1 latency
977 and rebound. *Trends Immunol* 2023;**44**:60–71.
978 35 Wei P, Garber ME, Fang S-M, Fischer WH, Jones KA. A novel CDK9-associated C-type cyclin
979 interacts directly with HIV-1 tat and mediates its high-affinity, loop-specific binding to TAR RNA.
980 *Cell* 1998;**92**:451–62.
981 36 Peng J, Zhu Y, Milton JT, Price DH. Identification of multiple cyclin subunits of human P-TEFb.
982 *Genes Dev* 1998;**12**:755–62.
983 37 Stoeckius M, Zheng S, Houck-Loomis B, Hao S, Yeung BZ, Mauck WM 3rd, *et al.* Cell Hashing
984 with barcoded antibodies enables multiplexing and doublet detection for single cell genomics.
985 *Genome Biol* 2018;**19**:224.
986 38 Weinreb C, Rodriguez-Fraticelli A, Camargo FD, Klein AM. Lineage tracing on transcriptional
987 landscapes links state to fate during differentiation. *Science* 2020;**367**:eaaw3381.
988 39 Vitak SA, Torkenczy KA, Rosenkrantz JL, Fields AJ, Christiansen L, Wong MH, *et al.* Sequencing
989 thousands of single-cell genomes with combinatorial indexing. *Nat Methods* 2017;**14**:302–8.
990 40 Yang D, Cho H, Tayyebi Z, Shukla A, Luo R, Dixon G, *et al.* CRISPR screening uncovers a central
991 requirement for HHEX in pancreatic lineage commitment and plasticity restriction. *Nat Cell Biol*
992 2022;**24**:1064–76.
993 41 Rosen BP, Li QV, Cho H, Liu D, Yang D, Graff S, *et al.* Parallel genome-scale CRISPR screens
994 distinguish pluripotency and self-renewal. *BioRxivorg* 2023.
995 https://doi.org/10.1101/2023.05.03.539283.
996 42 Li QV, Dixon G, Verma N, Rosen BP, Gordillo M, Luo R, *et al.* Genome-scale screens identify
997 JNK-JUN signaling as a barrier for pluripotency exit and endoderm differentiation. *Nat Genet*
998 2019;**51**:999–1010.

43 Thanasopoulou A, Stravopodis DJ, Dimas KS, Schwaller J, Anastasiadou E. Loss of CCDC6 affects cell cycle through impaired intra-S-phase checkpoint control. *PLoS One* 2012;**7**:e31007.
44 Morra F, Luise C, Merolla F, Poser I, Visconti R, Ilardi G, *et al.* FBXW7 and USP7 regulate CCDC6 turnover during the cell cycle and affect cancer drugs susceptibility in NSCLC. *Oncotarget* 2015;**6**:12697–709.
45 Zhou Y, Luo K, Liang L, Chen M, He X. A new Bayesian factor analysis method improves detection of genes and biological processes affected by perturbations in single-cell CRISPR screening. *Nat Methods* 2023. https://doi.org/10.1038/s41592-023-02017-4.
46 Dong M, Wang B, Wei J, de O Fonseca AH, Perry CJ, Frey A, *et al.* Causal identification of single-cell experimental perturbation effects with CINEMA-OT. *Nat Methods* 2023;**20**:1769–79.
47 Hart T, Brown KR, Sircoulomb F, Rottapel R, Moffat J. Measuring error rates in genomic perturbation screens: gold standards for human functional genomics. *Mol Syst Biol* 2014;**10**:733.
48 Morgens DW, Deans RM, Li A, Bassik MC. Systematic comparison of CRISPR/Cas9 and RNAi screens for essential genes. *Nat Biotechnol* 2016;**34**:634–6.
49 Bunne C, Stark SG, Gut G, Del Castillo JS, Levesque M, Lehmann K-V, *et al.* Learning single-cell perturbation responses using neural optimal transport. *Nat Methods* 2023;**20**:1759–68.
50 Li WV, Li JJ. An accurate and robust imputation method scImpute for single-cell RNA-seq data. *Nat Commun* 2018;**9**:997.
51 Lun ATL, Bach K, Marioni JC. Pooling across cells to normalize single-cell RNA sequencing data with many zero counts. *Genome Biol* 2016;**17**:75.
52 Sun T, Song D, Li WV, Li JJ. scDesign2: a transparent simulator that generates high-fidelity single-cell gene expression count data with gene correlations captured. *Genome Biol* 2021;**22**:163.
53 Hao Y, Hao S, Andersen-Nissen E, Mauck WM 3rd, Zheng S, Butler A, *et al.* Integrated analysis of multimodal single-cell data. *Cell* 2021;**184**:3573-3587.e29.
54 Lee K, Cho H, Rickert RW, Li QV, Pulecio J, Leslie CS, *et al.* FOXA2 is required for enhancer priming during pancreatic differentiation. *Cell Rep* 2019;**28**:382-393.e7.

Figures

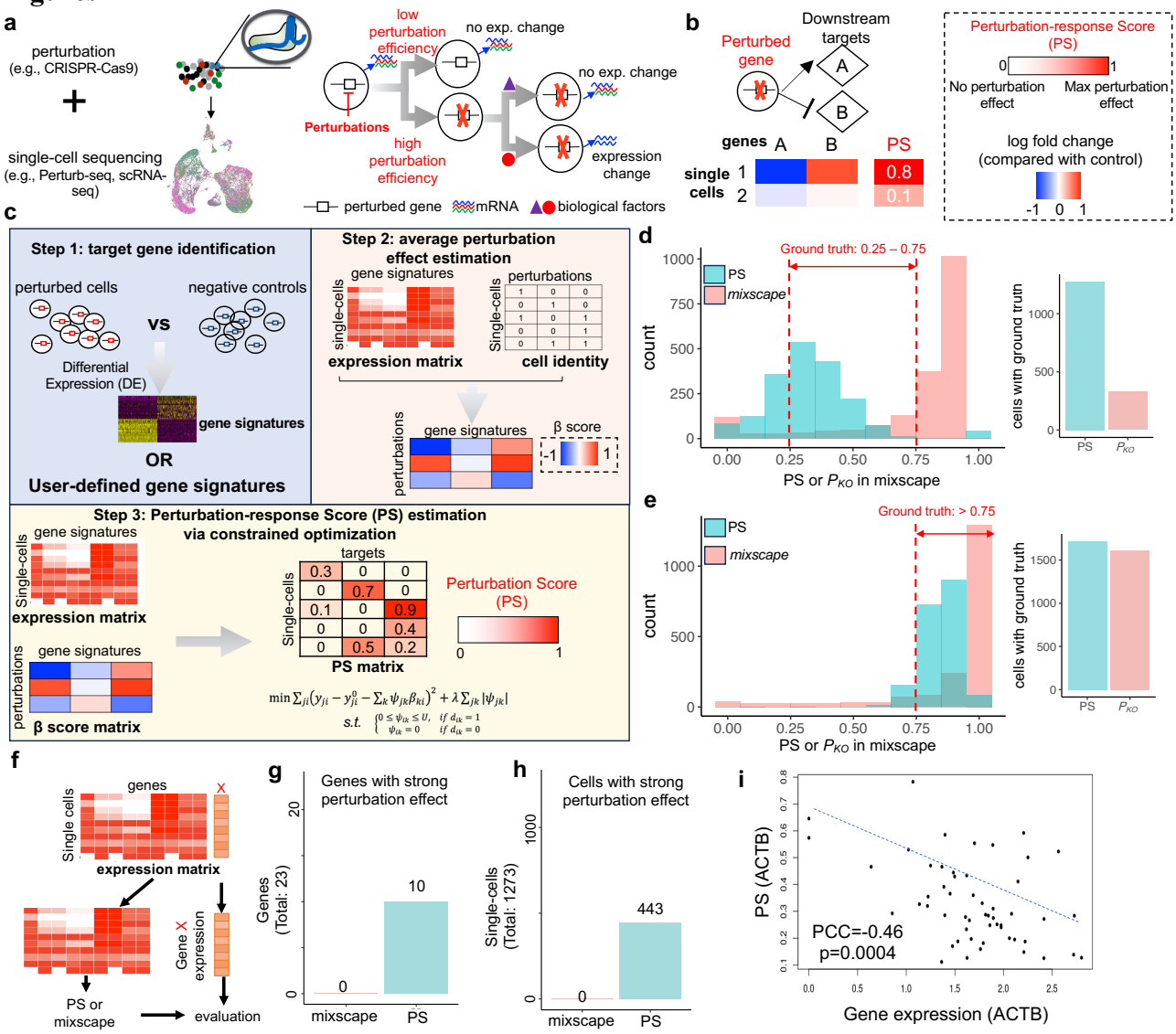

$$\min \sum_{ji}\left(y_{ji} - y_{ji}^{0} - \sum_{k}\psi_{jk}\beta_{ki}\right)^2 + \lambda \sum_{jk}|\psi_{jk}|$$

$$s.t. \begin{cases} 0 \le \psi_{ik} \le U, & if\ d_{ik} = 1 \\ \psi_{ik} = 0 & if\ d_{ik} = 0 \end{cases}$$

Figure 1. The Perturbation-response Score (PS) framework and benchmark. a, Overview of different technical and biological factors that contribute to heterogenous perturbation outcomes from single-cell perturbation datasets. **b,** Using downstream gene expressions to infer the value of PSs. **C,** Overview of the scMAGeCK-PS that estimates PS value. **d-e,** Benchmark results of both PS and mixscape using simulated datasets, where 50% (**d**) and 100% € gene perturbation effects are simulated using scDesign3. Here, the expressions of 200 differentially expressed genes (DEGs) from bulk RNA-seq (Nelf knockout vs. wild-type) are simulated, and ground truth efficiency value is indicated in red color. **f,** Benchmark pipeline using real CRISPRi-based Perturb-seq datasets, where the perturbation efficiency can be evaluated directly via gene expression. **g-h,** Benchmark results of mixscape and scMAGeCK-PS using a published Perturb-seq dataset, by counting the numbers of cells or genes with strong perturbation effects. A gene is considered to have strong perturbation effect, if a strong negative correlation (Pearson correlation coefficient < -0.1) is observed between PS and the expression of that gene across all perturbed cells. A cell is considered to be strongly perturbed, if its predicted efficiency score (by scMAGeCK-PS or mixscape) within one cell is greater than 0.5. The Perturb-seq experiment

is performed with low MOI condition, where most cells have only 1 expressed guide. **i,** An representative estimation results of scMAGeCK-PS and their correlations of ACTB expression.

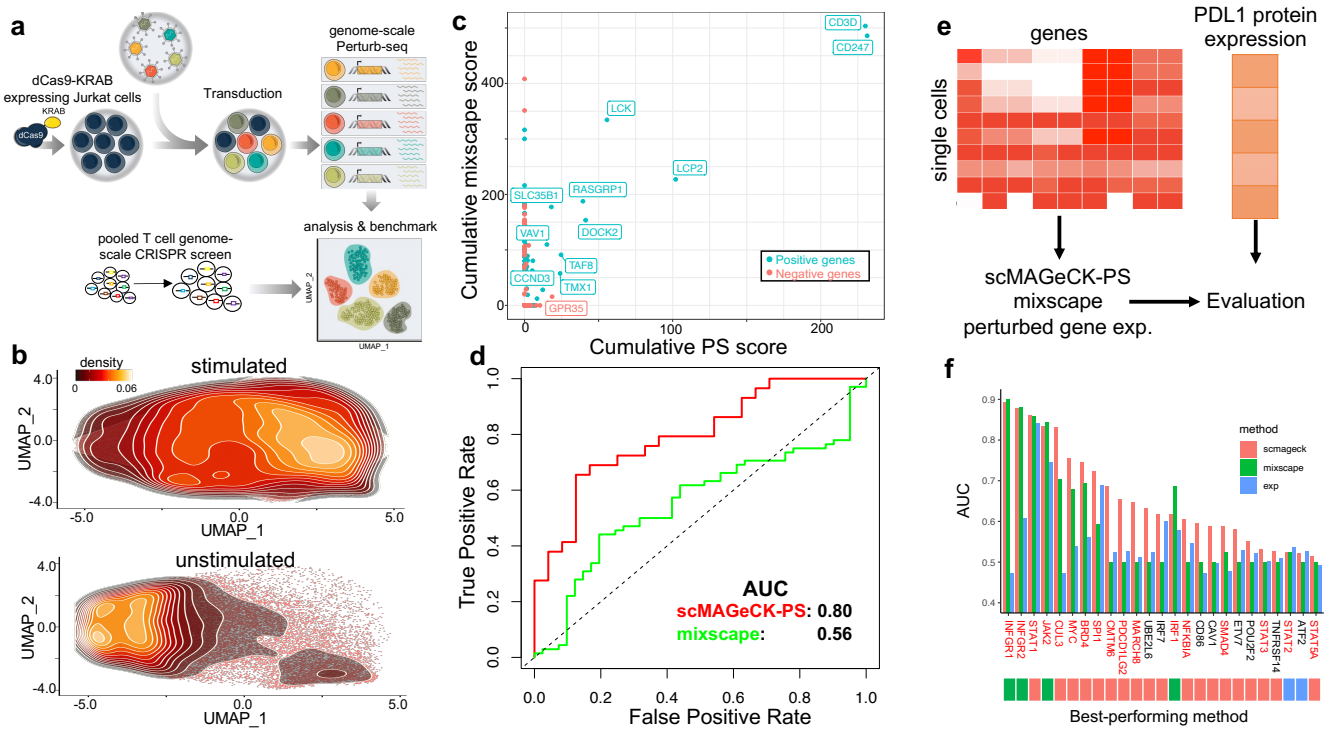

Figure 2. Additional benchmark results using genome-scale Perturb-seq and ECCITE-seq. a, Benchmark procedure using a genome-scale Perturb-seq and a published, pooled T cell CRISPR screen. **b,** The distribution of unstimulated and stimulated Jurkat cells along the UMAP plot. **c,** The correlation of predicted scores by scMAGeCK-PS and mixscape. **d,** the Receiver-Operating Characteristic (ROC) curve of both methods in separating positive and negative hits. **e-f,** Benchmark using a published ECCITE-seq where PDL1 protein expression is used as gold standard (**e**), and the performance of different methods in terms of predicting PLD1 protein expression (**f**).

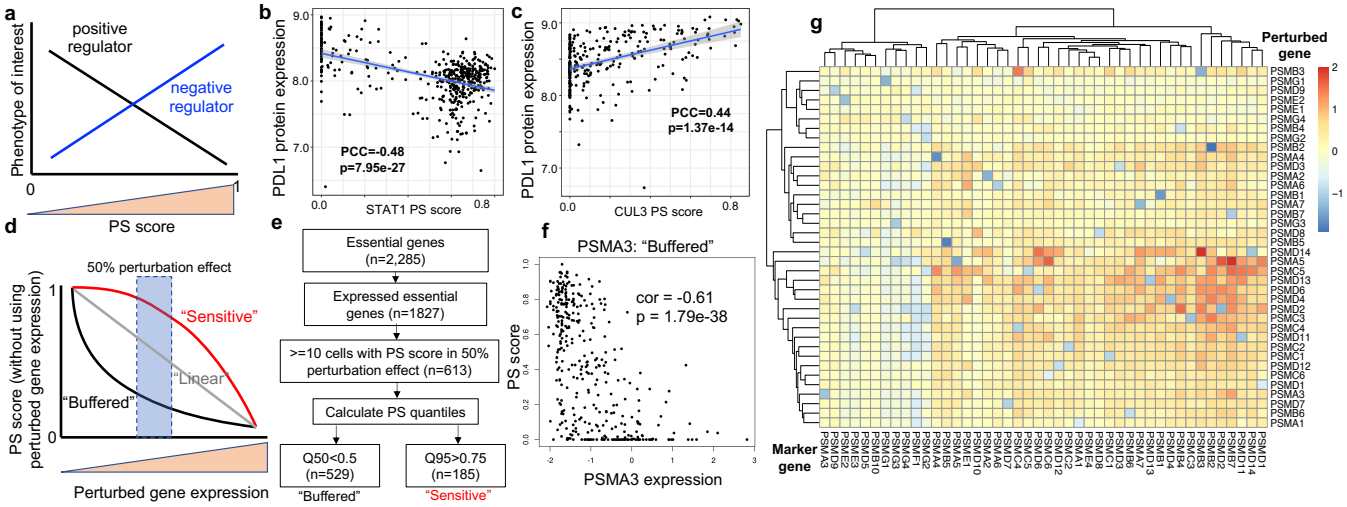

Figure 3. Dose-dependent responses of perturbations. a, The correlation between a gene's PS and a phenotype of interest indicates positive (or negative) regulations. **b-c,** The correlation between PDL1 protein expression and the PS of CUL3 (**b**) and STAT1 (**c**). CUL3 is a known negative regulator of PDL1, while STAT1 is a known positive regulator. **d,** The classification of buffered or sensitive genes, based on perturbed gene expression and PS. **e,** The classification of buffered or sensitive genes from published Perturb-seq datasets focusing essential genes in K562[26]. **f,** The perturbation-expression plot of PSMA3, a buffered gene. **g,** The log fold changes of mark gene expressions (columns) upon perturbing proteasome genes (rows) from the essential gene Perturb-seq dataset.

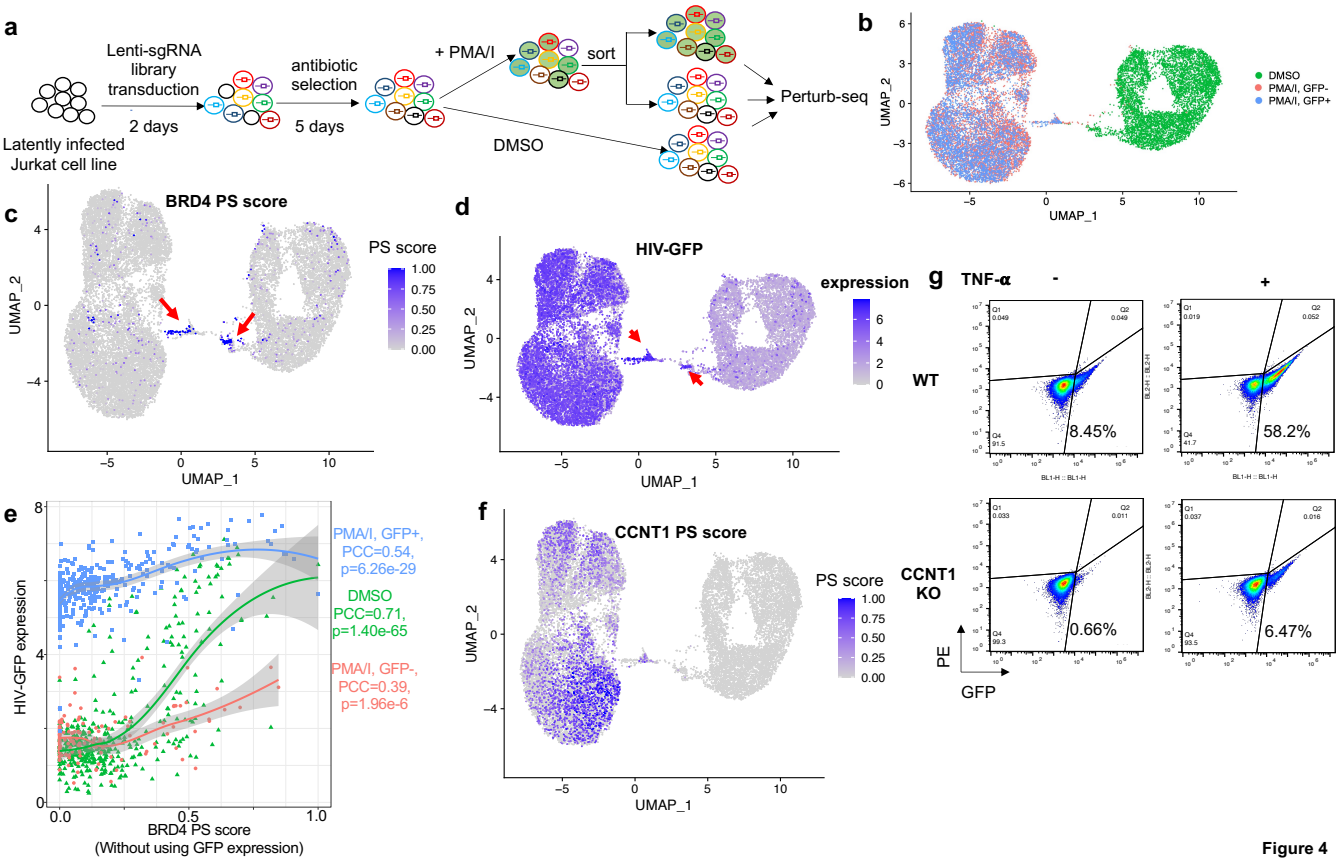

Figure 4

Figure 4. Perturb-seq on HIV latency. a, The experimental design of Perturb-seq. **b,** The UMAP plot of single-cell transcriptome profiles. Cells are colored by three different conditions. **c,** The distribution of BRD4 PS. **d,** The expression of HIV-GFP. **e,** The correlations between HIV-GFP expression and BRD4 PS that does not use HIV-GFP as target gene. **f,** The distribution of CCNT1 PS. **g,** The protein expression of HIV-GFP in response to CCNT1 knockout in different cell states (TNF-alpha vs non-stimulated).

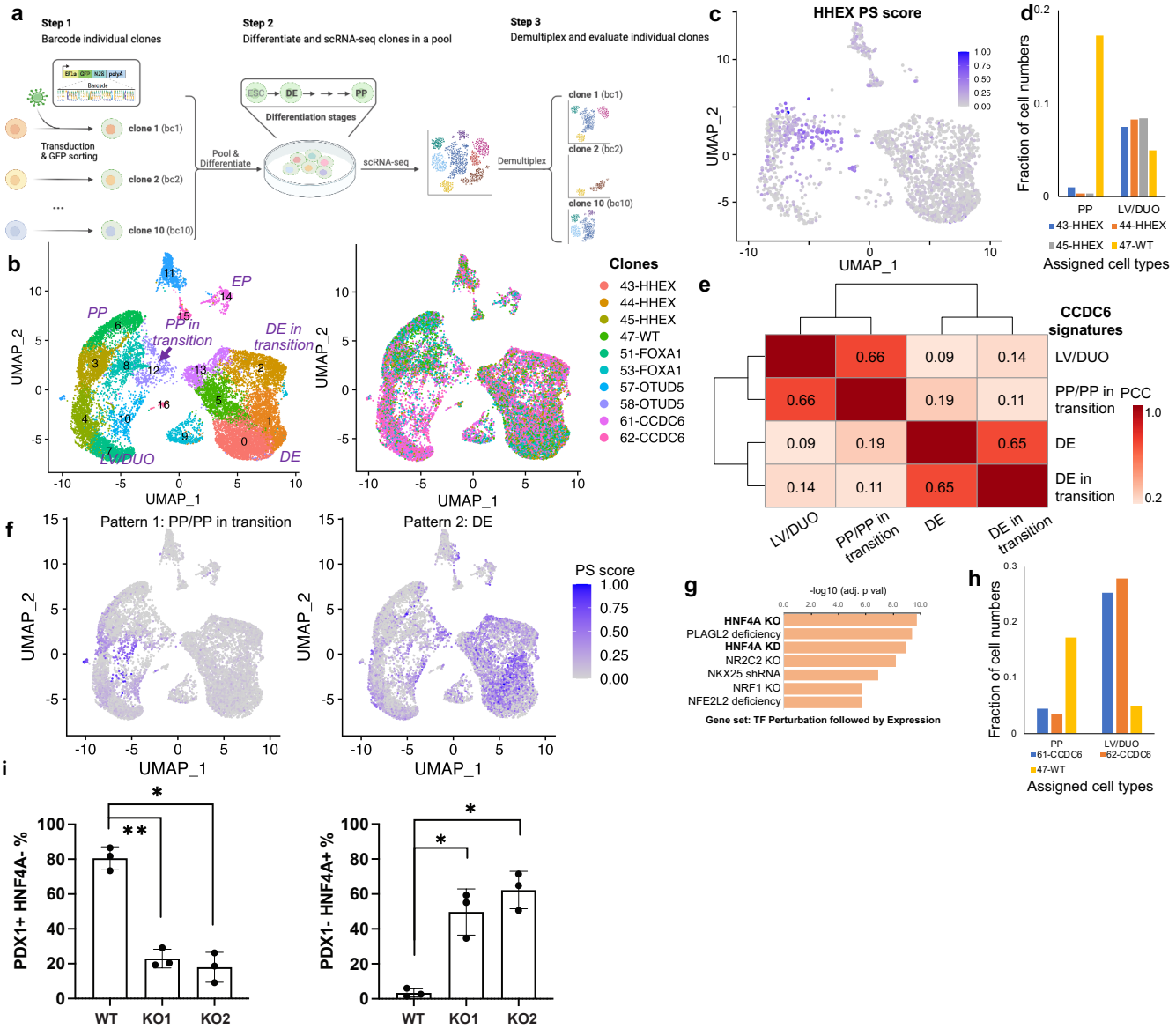

Figure 5

Figure 5. Pooled scRNA-seq on pancreatic differentiation. a, Experimental design of multiplexing scRNA-seq on the knockout clones of different genes. **b,** The UMAP plot of single-cell transcriptome profiles, colored by different clusters (left) or clones (right). **c,** The PS distribution of HHEX. **d,** The percentage of cells in PP/LV/DUO cell types from different clones. **e,** The correlations of CCDC6 PSs calculated from different HHEX cell types. The Pearson Correlation Coefficient (PCC) is calculated from all cells with CCDC6 knockouts and is shown as numbers on the heatmap. **f,** Two different distribution patterns of CCDC6 PSs. **g,** The top enriched GO terms of DEGs from PP/PP in transition. Enrichr was used to perform enrichment analysis. **h,** The percentage of cells in PP/LV/DUO cell types from CCDC6 clones. **i,** The percentage of cells with PDX1+ (a PP marker) or HNF4A+ (a LV marker) by flow cytometry sorting. The data is based on two CCDC6 knockouts (KO1, KO2) and one wild-type (WT) control. Three independent replicates are performed for each condition. The multiple comparison-adjusted p value is calculated by one-way ANOVA test. *p<0.05, **p<0.01.

1094 **Supplementary Figure Legends**
1095
1096 **Supplementary Figure S1. Benchmark different methods using simulated and real datasets. a,**
1097 Steps to generate simulated datasets using scDesign3 from a real scRNA-seq dataset that knocks out
1098 Nelfb gene. **b-e,** The score distribution of scMAGeCK-PS and mixscape using different DEGs and
1099 different values of true efficiencies. **f-g,** Similar with Figure 1f-g, but using a published high MOI
1100 Perturb-seq dataset in the same study. **h-i,** Benchmark results of different methods on another published
1101 CRISPRi-based Perturb-seq, where mismatches are introduced into guides to attenuate perturbation
1102 effects. The Pearson correlation coefficients (PCCs) between the predicted scores of each method and
1103 the expressions of perturbed genes are reported for every perturbed gene (**h**), and between the predicted
1104 scores and predicted sgRNA activities (**i**), using the prediction methods provided in the original study[21].
1105
1106 **Supplementary Figure S2. A genome-scale Perturb-seq. a-b,** The distribution of scMAGeCK-PS and
1107 mixscape predicted scores of top hits including CD247 (**a**) and LCK (**b**) in the pooled screen. **c,** The
1108 correlation between PSs and perturbed gene expression.
1109
1110 **Supplementary Figure S3. Predictions of PDL1 protein expression from a published ECCITE-seq**
1111 **dataset.** The ROC curve, the correlations between scMAGeCK-PS results with PDL1 protein
1112 expression, and the correlations between mixscape results with PDL1 protein expression are reported for
1113 each gene. The correlations are separated by classifications of each single cell: NP (non-perturbed),
1114 defined as mixscape score <=0.5; and KO (knockout), defined as mixscape score >0.5. For a fair
1115 comparison, we used mixscape classification results to plot PSs (mid panel).
1116
1117 **Supplementary Figure S4. Buffered genes and sensitive genes. a,** RPL4, a buffered gene. **b-c,**
1118 HSPA5 and GATA1, two sensitive genes. **d,** A gene (BRD4) whose expression has no correlation with
1119 PS.
1120
1121 **Supplementary Figure S5. The log fold changes of gene expressions upon perturbing genes within**
1122 **the same protein complex**, including ribosomal subunits (**a**), RNA polymerase (**b**) and mediator
1123 complex (**c**) in essential gene Perturb-seq. **(d)** The log fold changes of proteosome gene expressions
1124 (columns) upon perturbing proteasome genes (rows) from the genome-scale Perturb-seq.
1125
1126 **Supplementary Figure S6. HIV Perturb-seq. a,** The number of genes (nFeature_RNA), UMI counts
1127 (nCount_RNA) and the fraction of mitochondrial RNAs in three different conditions. **b,** Clustering
1128 results. **c,** Enriched Gene Ontology (GO) terms of cluster 8. **d,** The distribution of BRD4-targeting
1129 gRNAs. **e,** The expression distribution of BRD4 signature genes in cluster 8 vs other clusters. Only cells
1130 express BRD4-targeting gRNAs are included. **f,** Differential expression results between BRD4 PS+ cells
1131 vs BRD4 PS- cells.
1132
1133 **Supplementary Figure S7. HIV Perturb-seq. a,** The expressions of CCNT1 (left) and CCNT1-
1134 targeting gRNAs (right). **b,** Differential expression results between CCNT1-targeting cells and non-
1135 targeting control cells in two different cell states. **c,** The expressions of NFKB1. **d,** The quantitative
1136 perturbation-expression relationship between GFP and CCNT1 PS, similar with Figure 4e.
1137
1138 **Supplementary Figure S8. Cell type assignment based on known expression markers of different**
1139 **cell types in pancreatic differentiation scRNA-seq.**

1140
1141 **Supplementary Figure S9. DEG analysis.** a**-b,** The distribution of FOXA1 PSs across two different
1142 clones. **c,** The expression pattern of FOXA1. **d-e,** The DEG analysis results of CCDC6 knockout clones
1143 vs. wild-type clones in different cell types. **f,** The overlap of statistically significant DEGs in DE and
1144 LV/DUO cell types.
1145
1146 **Supplementary Figure S10. Different CCDC6 functions. a-b,** The two patterns of CCDC6 PSs in
1147 LV/DUO (**a**) and DE in transition (**b**) cell types. **c-f,** Additional enriched terms using Enrichr on DEGs
1148 of CCDC6 knockout.
1149
1150 **Supplementary Figure S11. Flow cytometry analysis of PDX1 and HNF4A expression upon**
1151 **CCDC6 knockout.** One representative plots of three biological replicates are shown.
1152
1153 **Supplementary Table S1. Genome-scale Perturb-seq library design.**
1154
1155 **Supplementary Table S2. HIV Perturb-seq library design.**
1156
1157 **Supplementary Table S3. Sequencing summary of HIV Perturb-seq.**
1158
1159 **Supplementary Table S4. Genotype summary of 10-clone scRNA-seq pancreatic differentiation**
1160 **dataset.**